



Pioneering Spirit Jacket Lift System

A dynamic analysis of the jacket mating loads
E.R. Kuiters

Technische Universiteit Delft

Pioneering Spirit Jacket Lift System

A dynamic analysis of the jacket mating loads

by

E.R. Kuiters

to obtain the degree of Master of Science
at the Delft University of Technology,
to be defended publicly on Tuesday September 4, 2018 at 2:00 PM.

Student number:	4096169
Project duration:	Sept 1, 2017 – September 4, 2018
Thesis committee:	Prof. dr. ir. A. P. van 't Veer, TU Delft
	Dr.ir. P. R. Wellens, TU Delft
	Ir. H. Bailly Guimaraes, Allseas
	Dr.ir. A. Vrijdag, TU Delft

This thesis is confidential and cannot be made public until September 2023.

An electronic version of this thesis is available at <http://repository.tudelft.nl/>.

Preface

This report is the result of my thesis performed to complete my master Offshore & Dredging Engineering at Delft University of Technology. My sincere thanks to Allseas Engineering B.V. for giving me the guidance, tools and support to graduate.

I would like to express my gratitude to the members of my graduation committee, Riaan van 't Veer, Peter Wellens, Helio Bailly Guimaraes and Arthur Vrijdag, for giving me the opportunity to obtain my Masters degree. I want to thank Professor van 't Veer for asking all the critical questions and giving valuable input during the meetings we had. I would like to especially thank Peter, my daily supervisor at the TU, for having endless patience with me, the structured meetings and for always providing good advise. I would also like to express special gratitude to Helio, my supervisor at Allseas, for giving me with the right guidance, support and valuable insights during the course of my thesis.

Many thanks as well to my brothers Thade en Friso, my parents, my friends and fellow graduates at Allseas for the support and motivation.

E.R. Kuiters
Delft, September 2018

Abstract

Allseas Engineering B.V. is an offshore contractor, focussed on offshore pipeline installation. Since the late 80's, Allseas has been working on the design and construction of the *Pioneering Spirit*, a heavy lift vessel designed for the single-lift installation and removal of offshore topsides. From 2019, it is scheduled to be able to single-lift install or remove jackets with the jacket lift system.

The jacket lift system is located at the aft of the vessel and consists of two 170 meter tilting lift beams, hinged around the stern. During a jacket removal, the jacket is cut-off at the bottom, hoisted from the tip of the beams, partially rotated, and then tilted inboard. In between the hoisting and tilting is the transition phase. At the interface between jacket and the tilting lift beams, jacket support structures are located. In this thesis, the behaviour of the free-hanging of the jacket and the loads on these support structures due to the mating with the jacket are researched.

Jacket removal operations will take place in open sea and are thus subjected to environmental actions. The jacket, suspended from the tip of the beams, is excited due to fluid acceleration and velocity causing inertia forces and predominantly drag forces on the slender members of the jacket, as well as the excitation of the vessel through the suspension point. These motions are calculated with two different approaches. A direct-time domain model is developed of the jacket as submerged pendulum. To accelerate model simulations, the jacket is modelled as one single cylinder with different equivalent diameters to account for the total of drag and inertia. The second model is a full geometrical time-domain model simulation in AQWA.

In the design sea state, simulations showed that the most probable maximum momentum of the jacket due to environmental excitation is $4.5 \cdot 10^6$ kg m/s, and the motions of the centre of gravity of the jacket are all within a range of 1 meter, for the single and double pendulum and the full model. The influence of the environmental actions on motions of the structure is concluded to be small. This suggest that that jacket mating loads are governed by the tilting velocity of the tilting lift beams and the motion of its tip. The jacket mating simulations are done in the full AQWA model approach.

Fenders are modelled to absorb energy during the jacket mating. A sensitivity analysis showed that the parameters that have most influence on the mating phase characteristics are the tilting velocity and the stiffness of the fender. From still water conditions it seems that by increasing *or* decreasing the tilting velocity, this can affect the number of re-bounces and the maximum deflection. With increasing sea state, the duration and intensity of the mating phase increases. The fender deflection will increase for increasing significant wave height. The wave period does not have an significant influence on the maximum fender force. The amount of re-bounces reduces significantly for higher damping coefficients, while its influence on maximum deflection decreases.

The maximum force on the jacket support structures caused by the static gravitational force by the jacket once it is fully tilted, is approximately 10 times higher than the maximum occurring force exerted on one of the fenders. Therefore, this static gravitational force is critical for the design of the jacket support structure, not the force caused by the mating.

Nomenclature

Abbreviations

COG	Centre of Gravity
COR	Coefficient of Restitution
DNV-RP	Det Norske Veritas - Recommended Practice
DOF	Degree of Freedom
FD	Frequency Domain
HOF	Hang-off Frame
GEA	Guaranteed Energy Absorption
JLS	Jacket Lift System
JONSWAP	Joint North Sea Wave Project
MSWL	Mean Sea Water Level
PM	Pierson-Moskowicz
PS	Pioneering Spirit
RAO	Response Amplitude Operator
RK	Runge Kutta
SB	Starboard
TD	Time Domain
TLB	Tilting Lift Beam
TLS	Topside Lift System

Symbols

Symbol	Unit	Description
θ_{TLB}	rad	tilting angle of TLB
H_s	m	significant wave height
T_z	s	Zero-mean wave crossing period
T_p	s	Peak period
μ	deg	wave direction
θ	rad	single pendulum angle
$\dot{\theta}$	rad/s	single pendulum angular velocity
\mathcal{L}		Lagrangian multiplier
ω_n	rad/s	natural frequency
θ_1	rad	upper angle wrt y-axis double pendulum
θ_2	rad	lower angle wrt y-axis double pendulum
σ		standard deviation
ρ	kg/m ³	density
C_m		inertia coefficient
C_d		drag coefficient
ζ	m	wave amplitude
ω	rad/s	wave frequency
α		linearisation factor
α_{TLB}	m/s	tilting velocity of TLB tip
η	m	surface elevation
ϵ		phase
e^*		coefficient of restitution
ν	m ² /s	kinematic viscosity

Conventions

Global Coordinate System

The global coordinate system of the *Pioneering Spirit* is defined as follows (figure 1):

- X-axis (from aft perpendicular) in longitudinal vessel direction pointing forward.
- Y-axis (from centreline) in transverse vessel direction pointing portside
- Z-axis (from bottom line) in vertical direction pointing upward

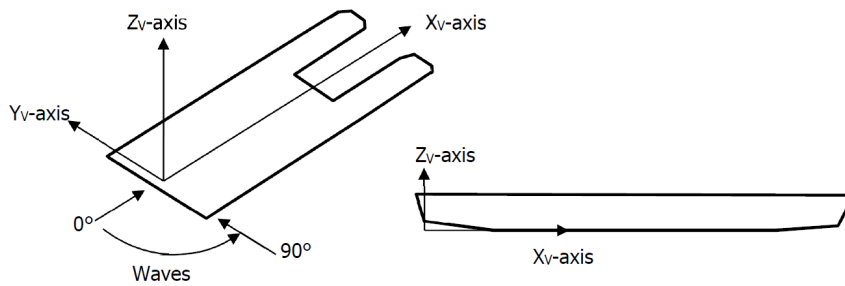


Figure 1: Global vessel coordinate system

Vessel Motion Coordinate System

The vessel motions are defined relative to the Centre of Gravity (CoG) of the vessel. Surge, Sway and Heave are translational motions. Roll, Pitch and Yaw are rotational motions (figure 2)

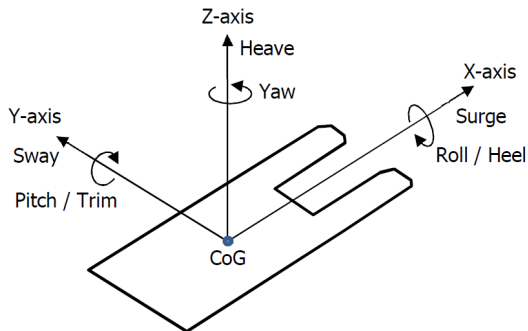


Figure 2: Vessel motion coordinate system

Contents

Preface	iii
Abstract	v
1 Introduction	1
1.0.1 Allseas	1
1.0.2 Pioneering Spirit	1
1.0.3 Jacket Lift System	2
1.1 Subject Definition.	3
1.1.1 Research question and scope	3
1.1.2 Research methodology.	3
2 Equipment and boundary conditions	5
2.1 Vessel	5
2.2 Jacket Lift System	6
2.3 Jacket	7
2.4 Load cases	8
2.4.1 Environmental load cases	9
2.4.2 Geometrical load cases.	9
3 Literature review	11
3.1 Frequency Domain	11
3.2 Time Domain	13
3.3 Morison forces	16
3.3.1 Morison force integration over a structure	16
3.3.2 Wheeler stretching	17
3.3.3 Vector calculations.	18
3.4 Wave record generation.	18
3.5 Impact	20
3.6 Fenders	22
4 Model Design	25
4.1 MatLab model	25
4.1.2 Motion influences of jacket	27
4.2 Jacket representation	31
4.2.1 Equivalent Stick Model.	31
4.2.2 Equivalent Cylinder	33
4.3 AQWA model	33
4.3.1 Relative vs. Absolute Velocity approach in Frequency domain approach.	35
5 Simulation results	37
5.1 Structure motions.	37
5.2 Impact	41
5.2.1 Static behaviour fender	43
5.2.2 No Environmental forces.	44
5.2.3 With environmental forces.	47
5.3 Geometrical Loadcases	49
6 Conclusions	53
6.1 Conclusions.	53
6.2 Recommendations	54

List of Figures	55
List of Tables	57
Appendix A: Personal information	59
Appendix B: Simulation results	61
Appendix C: Fender characteristics	65
Appendix D: Jacket Installation/Removal configuration	67
Appendix E: MatLab model verification	69
Bibliography	73

Introduction

This chapter introduces this thesis' subject to the reader. This thesis is made within the innovations department of Allseas Engineering BV Delft, from now on called Allseas. This chapter starts with a brief introduction into the company and the concerned vessel for this thesis. This is followed with an introduction in the research question, the corresponding sub questions and the research methodology.

1.0.1. Allseas

Allseas is an offshore contractor, focused on offshore pipeline installation, heavy lift and sub sea construction. It was founded in 1985 by Edward Heerema, who still is in charge of the company. Allseas has over 2500 employees, and its history is marked by many technical novelties, which is made possible by their relatively large innovation department. It is one of the first companies to use Dynamic Positioning during pipe laying, which is regarded as a major cost and time improvement in offshore pipe laying industry. Allseas' main expertise has been offshore pipe laying since the establishment of the company, though as of 2015, it added heavy lift to its portfolio with the completion of the *Pioneering Spirit* (formerly the Pieter Schelte).

1.0.2. Pioneering Spirit

The *Pioneering Spirit* (PS) is a twin-hulled multi-purpose vessel that is 382 m long and 124 wide, making it one of the largest construction vessels built. It was delivered in 2015. With its large dimensions and its unconventionally fork-shaped hull, it has some unique functionalities. Most significant is that it can remove and install a topside in a single lift, while actively compensating for vessel and wave motions. It has proven the functionality of this Topside Lifting System (TLS) in May 2017 with the successful removal of the 24.000 tonnes Brent Delta topside in the North Sea, and in June 2018 with the successful installation of the 22.000 tonnes Johan Sverdrup topside (figure 1.1). In addition, the PS is used for pipe laying in deep water, when it is not used for topside lifting.



Figure 1.1: *Pioneering Spirit* with Johan Sverdrup topside (2018)

1.0.3. Jacket Lift System

After the proven concept of TLS, one of the new challenges for the PS, scheduled for around 2019, is the removal of a jacket or tower¹ using the Jacket Lifting System (JLS). The OSPAR Convention ([1], annex III) of 1992 states guidelines and rules on the protection and elimination of pollution from offshore sources in the North-East Atlantic. Herein is stated that the contracting parties shall require the use best available techniques and best environmental practice during installation, operational lifetime and decommissioning. Allseas is aiming to meet this demand with the construction of the JLS.

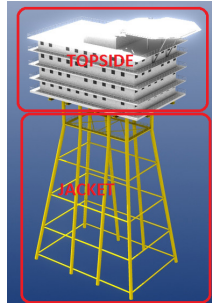


Figure 1.2: Layout of typical offshore structure

The main two components of the JLS system are the Tilting Lift Beams (TLBs). These 170 meter beams are hinged at the aft of the vessel, rotating around the y-axis. The tip of the TLBs are attached to the derrick hoist system, a system of cables, sheaves and winches that allow the TLBs to rotate. The tip of the Tilting lift beam is connected with a system of sheaves and hoisting wires, with a jacket that is to be decommissioned. By means of underwater cutting devices, the jacket is cut-off near the sea bottom. By continuously hoisting the jacket and the derrick hoist system, the jacket is lifted and rotated by varying winching velocity of aft and front side hoisting cables that are connected to the jacket. By winching in the derrick hoist system, the jacket mates with the jacket support structures, or 'grillages'. Consequently it is levered it on the aft deck of the PS. After that, the jacket will be transferred to shore, by means of barge or directly. Vice versa, the installation of a jacket is also possible. In upended position, the JLS can also be used as a multi-purpose crane. In figure 1.3 is a schematic overview of a jacket removal procedure is given.

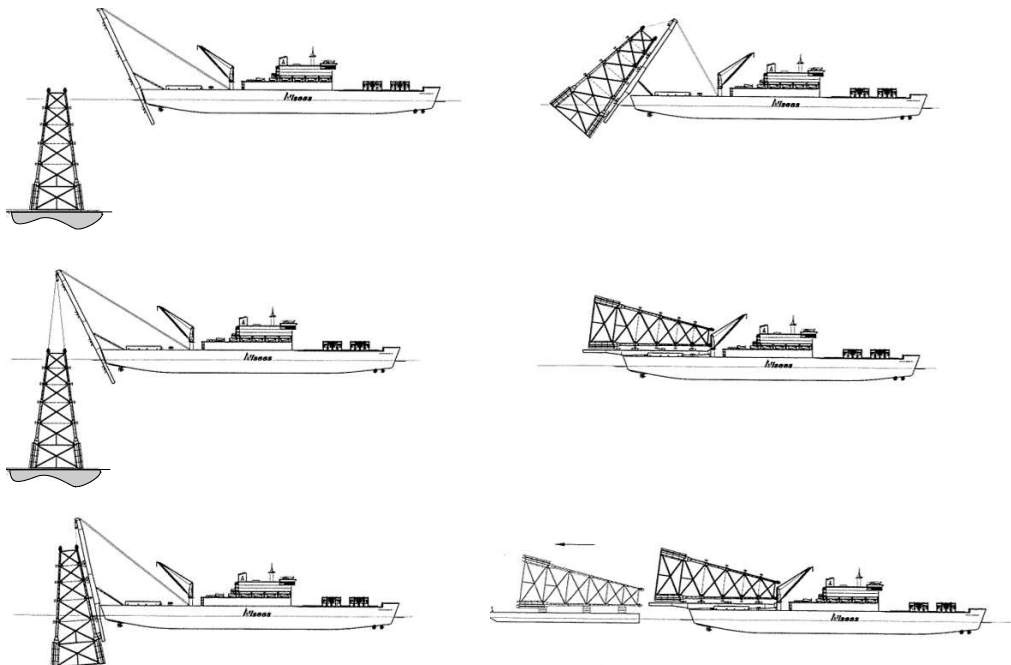


Figure 1.3: Schematic view of how the JLS works

¹from here on there will only be referred to jackets, while in general both tower and jackets can be meant

For this thesis, the JLS jacket removal procedure can be separated in three different phases:

- **Lifting phase.** This phase starts when the jacket is hoisted and tilted so that the inclination of the jacket matches the inclination of the TLBs. The phase ends when the jacket starts to make contact with the TLBs.
- **Transition phase.** During this phase, also referred to as jacket mating phase, the TLBs are rotated inwards, causing the jacket to make initial contact. The impact loads during these loads are the jacket mating loads. This phase ends when this contact is continuous.
- **Tilting phase.** After there is continuous contact with the TLBs, the jacket is tilted further on the aft of the deck. More supports on the TLB for the jacket are activated

A more extensive description of the JLS is given in chapter 2.

Currently, the JLS system is in advanced design state. Most components are designed and built in-house by Allseas.

1.1. Subject Definition

Several dynamic models were made for the initial lift phase [2], of the JLS, when the jacket would detach from the sea bottom. Now, a more extensive analysis of the transition phase of the JLS is desired for the design of the jacket support structures.

The motivation for this thesis is to improve structural design for the JLS system during jacket removal, in particular during the transition phase. The mating of the two large structures, even with small velocity, can cause large forces, if the interface is not well designed. If the energy is not well absorbed, high impact forces can occur, which are among the most severe sources of vibration in vessels [3].

1.1.1. Research question and scope

To clarify the aim of this thesis, a research question is formulated. This is:

What are the key influences on the dynamic behaviour of the jacket mating loads on the Pioneering Spirit during the transition phase.

This research question is divided into several sub-questions:

- How can both bodies, i.e. the jacket and the vessel, be described dynamically?
- How are these bodies coupled and how can this combined system be approximated by a model?
- How can the jacket mating loads be approximated, when the jacket makes contact with the vessel?
- What are the most important external influences on the jacket lift system and how can these be integrated??

The focus of this research is *only* the transition phase. This excludes all operations prior to jacket mating, i.e. the attachment of the hoisting wires, cutting of the jacket legs and pre-tensioning the wires. All operations after the jacket has made continuous contact with the TLBs are also excluded. That includes the in-board tilting, skidding-in the jacket until it is lying on the aft of the vessel and sea fastening.

1.1.2. Research methodology

This research focuses on studying the dynamic behaviour of multiple bodies in irregular sea states, varying parameters to investigate which parameters have the most influence. Numerical and analytical methods will be used to determine worst case motions and therefore required energy absorption on relevant structures. If these can be accurately estimated, or conservative at least, structure damage can be prevented. Results of this report can be taken into account in the design of the interface between jacket and vessel. The research methodology is schematically given in figure 1.4.

A schematic overview of the proposed methodology is given in figure 1.4.

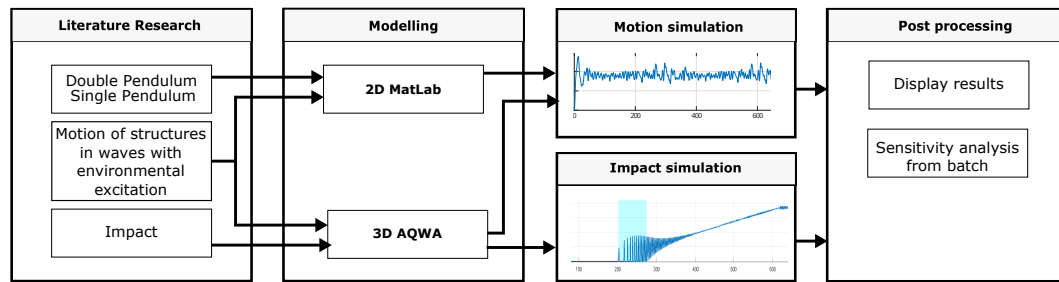


Figure 1.4: Research methodology

As mentioned, the jacket lift system is advanced design state, but has not yet been built. Also, there have not been conducted scale model tests yet of this system. This is very expensive and time-consuming. One alternative for real scale model testing is an CFD simulation, which also cost a lot of computational power, time and money. Therefore, this thesis aims to provide a alternative model, so the behaviour of the system can be predicted. This will be done by making a model in MatLab and using ANSYS AQWA².

- **MatLab** The system is modelled in a analytical model, to make system behaviour and the influence due to system parameters easier and quicker to investigate. The focus of this model will be mainly to accurately predict motions of the jacket. It will be built up from scratch and all the relevant physics and corresponding assumptions will be elaborated in subsequent chapters.
- **Ansys AQWA.** This is an existing engineering toolbox to research the effect of wave, wind and current effect on floating marine structures. It can calculate complex hydrodynamic analyses and motions responses. It simulates linearized hydrodynamic fluid wave loading on rigid bodies, by using diffraction and radiation theory on large bodies, and Morison equations on slender structures. It will be used to verify the previous mentioned MatLab model and to model impact as fenders

²from now on referred to as only AQWA

2

Equipment and boundary conditions

In this chapter, the structures, systems and procedures are described, that are relevant to start designing a model. At the end of this chapter, also the environmental and geometrical load cases that will be used are given and explained.

2.1. Vessel

The *Pioneering Spirit* (PS) is the largest vessel in Allseas' fleet. Its main deck stretches 382 meters long and 124 wide and it is designed for the removal or installation of offshore platform with a single lift. It is self propelled by 12 thrusters; 3 in each bow and 6 at the aft.

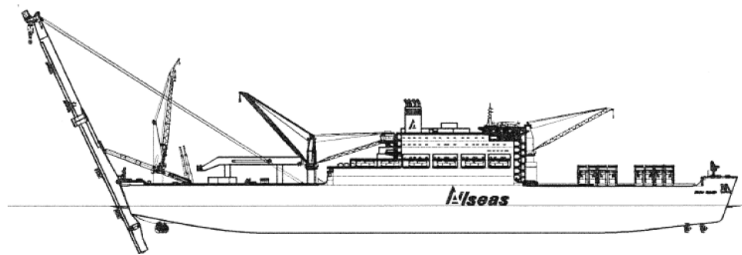


Figure 2.1: *Pioneering Spirit* in JLS configuration

The main dimensions of the vessel can be found in table 2.1

Item	Value	Unit
Length hull overall	382	[m]
Length between perpendiculars	370	[m]
Breadth moulded	124	[m]
Max depth	30	[m]
Draught, transit	11.5	[m]
Draught, pipelay	8.5	[m]
Draught, operational	17-22	[m]

Table 2.1: General dimension *Pioneering Spirit*

	X [m]	Y[m]	Z[m]
CoG PS	182.38	3.92	22.71

2.2. Jacket Lift System

The Jacket Lift Systems' two most important components are the Tilting Lift Beams (TLBs). Their length stretch 170 meters, and they have a mean cut section of around 140m². Both identical beams are hinged around the aft of the deck, at the Hang-Off Frame (HOF). These structures serve as hinge as well it houses a sheaves arrangement for the main hoist system.

A schematic overview of the JLS and all relevant parts can be seen in figure 2.2

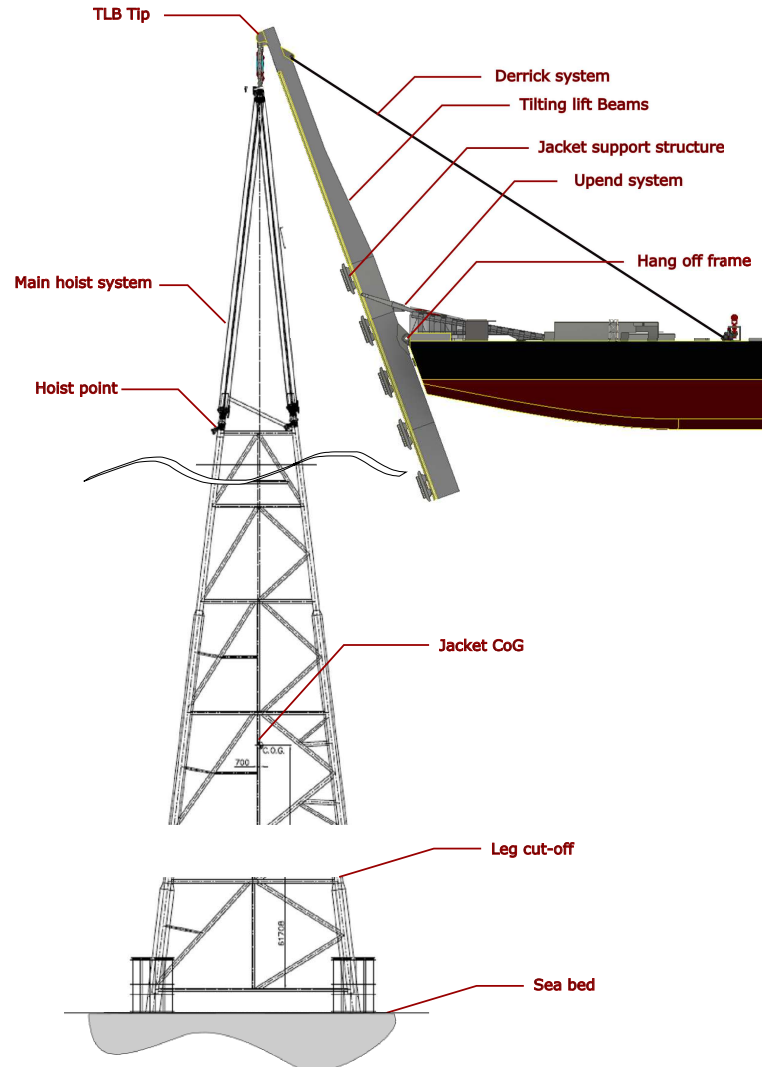


Figure 2.2: Schematic overview of Jacket Lift System

The removal of jacket is divided in several steps, which are described below [4].

1. Offshore preparations

- Jacket preparations; installation of the connection tool on the jacket top.
- Jacket leg cutting just above the seabed
- Select appropriate weather window.

2. TLB Outboard tilting

- By using the ppend system the TLBs are initially tilted, followed by tilting under heavy ballast in combination with ballast tanks, to an maximum angle of angle of 150°

3. Jacket inboard lifting

- Vessel positioning
 - Hoisting block connection to the jacket top
 - Apply pre-tension while ballasting PS to even keel position
 - Vertical lift. Base case is vertical lift; however, a tilted lift can also be executed if desired due to soil suction or complex jacket geometry. Lifting with predetermined time interval to flush jacket members. Heading change optional if desired.
 - During lift operations, the vessel is continuously ballasted, to even the keel trim.
 - Continuously measure CoG jacket with hoisting system and check structural integrity of jacket. During the hoisting the jacket is rotated by varying the winching velocity of the cables connected to the rear side of the jacket wrt the front side cables.
 - Mate jacket with tilting lift beams at the jacket support structures, the so called jacket transition phase
 - Skidded lift, alternating push-pull operations.
 - Inboard tilting
4. Prepare for transport
- Inboard skidding to transport position
 - Secure jacket to vessel deck
 - Retrieval hoisting blocks

The centre of gravity of one TLB is defined with respect to HOF, at an inclination of 0 degrees. Therefore, to obtain the correct COG, the coordinates are multiplied by a linearised rotation matrix \mathbf{R} , where θ_{TLB} is the pitch rotation at the HOF, and consequently these coordinates are translated to to global coordinate system.

$$\mathbf{R} = \begin{bmatrix} \cos \theta & -\sin \theta \\ \sin \theta & \cos \theta \end{bmatrix} \quad (2.1)$$

	X [m]	Y[m]	Z[m]
CoG PS	182.38	3.92	22.71
CoG TLB Tip (SB)	-45.02	0	8.52

Table 2.2: TLB Centre of Gravity

During jacket lift operations, the following conditions apply:

Item	Value	Unit
Draught	17	[m]
Max heel	1	[°]
Max trim	1	[°]

Table 2.3: Lift operations conditions

2.3. Jacket

Several design jackets are identified for the design of the JLS, that fulfil several functional requirements for decommissioning. The selection of these jackets is not within the scope of this thesis.

The gross weight of a jacket is divided in several subcategories:

- **Primary steelwork** All main structural items that contribute to the structures' integrity. Corrosion is not included.
- **Secondary steelwork** The weight of all components that do not contribute to the structure's integrity, such as ladders, walkways, caissons, conductor guide frames, stiffeners, etc.

- **Piles and Grout** The through-leg and skirt piles are a considerable part of the total weight. However, since jackets to-be-decommissioned are cut off above these base, these are not taken into account in the decommissioning load cases.
- **Marine growth** Submerged piles have an increased diameter due to marine growth. In case of slender member, this should be accounted for. The thickness depends on location and depth.
- **Entrapped water** Many of the jacket members are flooded. During hoisting, this entrapped water is assumed to have enough time to escape in order to not affect the hoisting operation.



Figure 2.3: Location of jacket in North Sea

From the design jackets, the Marathon Brae Bravo jacket is chosen as main design jacket, since its net removal weight is the highest of the design jackets [5]. The dimensions of the Brae jacket can be seen in figure 2.4, where the yellow sphere indicates the centre of gravity at [0, 0, 55]. In figure 2.4, the centre of the coordinate system is at the lowest Z-coordinate, in the centre of the X-Y plane. Due to lack of detailed structural data of most of the jackets, an other stick model of an other jacket (Forties jacket) is scaled to fit the Brae jackets' dimensions. The influence of this scaling is verified in a later chapter.

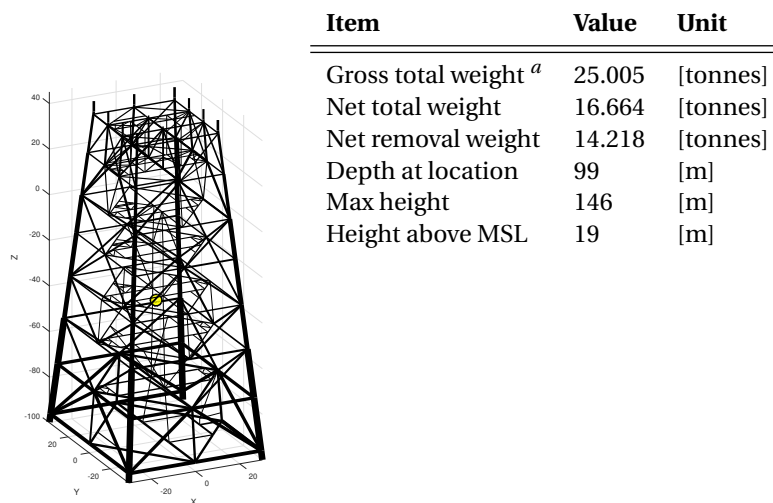


Figure 2.4: Jacket Properties

^aincluding part below cut

2.4. Load cases

Multiple load cases are determined, for which environmental or geometrical parameters vary. Simulation with these load cases help to understand which parameters have a significant influence on the JLS system.

2.4.1. Environmental load cases

The design load case of environmental parameters is based on the operational limits of the *Pioneering Spirit*. These parameters are given in table 2.4.

Parameter	Symbol [unit]	Operational Limit	Explanation
Significant wave height	H_s [m]	2.5	Mean wave height of the highest 1/3 waves
Wave period	T_z [s]	5.7	Time to complete one cycle of wave
Wave direction wrt vessel	μ [deg]	0 (stern)	Positive wave angel is counter-clockwise around ship
Current velocity	u_c [m/s]	0.5	-
Spectrum type	-	PM	Pierson Moskowitz wave spectrum

Table 2.4: Operational limit JLS

The Pierson Moskowicz spectrum is used as standard wave spectrum, because the energy in the sea state is more evenly distributed over the frequencies, while for the JONSWAP it is more concentrated around the peak period. This is more preferable in this model because the (yet) unknown natural frequencies have higher probability of being excited and therefore identified. Also, the design jacket is located in open sea, as can be seen in figure 2.3.

The design case presented in table 2.4 is load case 2. Other environmental load cases are defined in table 2.5. The values are based on the operational limits of the Pioneering Spirit Topside Lift System.

Load case	Based on operational limit of	H_s [m]	T_z [s]	Current velocity u_c [m/s]	Spectrum
1	Transfer	1	4.5	0.5	PM
2	Installation	2.5	5.7	0.5	PM
3	Transport (no heading control)	6	8.5	0.5	PM
4	Transport (w heading control)	10	10	0.5	PM

Table 2.5: Environmental load cases

2.4.2. Geometrical load cases

The following geometrical parameters are taken into account in simulating the model:

- **Fender stiffness.** The design linear stiffness is $5 \cdot 10^5$ kN/m.
- **Fender damping.** The design damping coefficient is 0.01 .
- **Tilting velocity.** The velocity at which the beams are tilted. This tilting is actuated by the the derrick hoist cable arrangement. The design velocity is 0.01 m/s of pulling the hoist wire. This equals approximately $9 \cdot 10^{-5}$ rad/s of rotational velocity of the tilting beam

3

Literature review

In this chapter, a literature and theory study is briefly described for all relevant aspects to model the Jacket Lift System.

3.1. Frequency Domain

When the jacket is suspended from the JLS, it shows characteristics with a suspended pendulum from a moving pivot. First, a frequency domain (FD) analysis is done, by assuming small angles for undamped pendulums.

3.1.1. Single pendulum

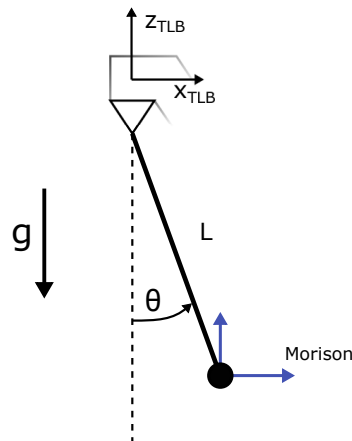


Figure 3.1: Pendulum model

The pendulum consists of a mass m is suspended from a ceiling with a massless rod, with length L . There is only one degree of freedom; the angle of θ with respect to the vertical axis. The pendulum is subjected to a gravitational acceleration of $g = 9.81 \frac{m}{s^2}$. The jacket is suspended from a pivot point, on which imposed motions are applied. For the frequency analysis, the pendulum is assumed undamped by fluid interaction (represented with blue arrows with 'Morison').

To calculate the equation of motion, first the position vector is determined. Its derivative in time gives the velocity vector

$$\mathbf{x} = X + L \sin \theta \quad (3.1)$$

$$\mathbf{z} = Z + L \cos \theta \quad (3.2)$$

$$\dot{\mathbf{x}} = \dot{X} + L \dot{\theta} \cos \theta \quad (3.3)$$

$$\dot{\mathbf{z}} = \dot{Z} - L \dot{\theta} \sin \theta \quad (3.4)$$

The equation of motion will be derived using the Lagrangian approach. First the kinetic energy and potential energy are defined. The kinetic energy is found as:

$$T = \frac{1}{2}Mv^2 = \frac{1}{2}M(\dot{x}^2 + \dot{z}^2) \quad (3.5)$$

$$= \frac{1}{2}M(\dot{X}^2 + \dot{Z}^2 + L^2\dot{\theta}^2 + 2L\dot{\theta}(\dot{X}\cos\theta - \dot{Z}\sin\theta)) \quad (3.6)$$

The potential energy is

$$V = mg \cdot z = mg(Z + L\cos\theta) \quad (3.7)$$

The Lagrangian is:

$$\mathcal{L} = T - V \quad (3.8)$$

$$\mathcal{L} = \frac{1}{2}mL^2\dot{\theta}^2 + mL\dot{\theta}(\dot{X}\cos\theta - \dot{Z}\sin\theta) + \frac{1}{2}m(\dot{X}^2 + \dot{Z}^2) - mgL\cos\theta - mgZ \quad (3.9)$$

Lagrange's equation is now solved:

$$\frac{d}{dt} \frac{\partial \mathcal{L}}{\partial \dot{\theta}} - \frac{\partial \mathcal{L}}{\partial \theta} = 0 \quad (3.10)$$

$$mL^2\ddot{\theta} + mL(g - \ddot{Z})\sin\theta + mL\ddot{X}\cos\theta = 0 \quad (3.11)$$

From equation 3.11 it can be deduced that for the undamped pendulum, if the pivot is moving, only its acceleration has influence on the pendulum's motion. In case we assume small angles, the equation of motion can be approximated with:

$$mL^2\ddot{\theta} + mg(L - \ddot{Z})\sin\theta + mL\ddot{X} = 0 \quad (3.12)$$

$$\ddot{\theta} = \frac{g(L - \ddot{Z})}{L}\sin\theta + \frac{1}{L}\ddot{X} \quad (3.13)$$

where the pendulum's natural frequency ω_n is found as the square root of the spring term as in equation 3.14. This only holds if $\ddot{X} = 0$ and $\ddot{Z} = 0$.

$$\omega_n = \sqrt{\frac{g - \ddot{Z}}{L}} \quad (3.14)$$

3.1.2. Double pendulum

The system will also be modelled as double pendulum as in figure 4.1. The equation of motion of the 2 DoF double pendulum is separated in two masses; the jacket and the hoisting block.

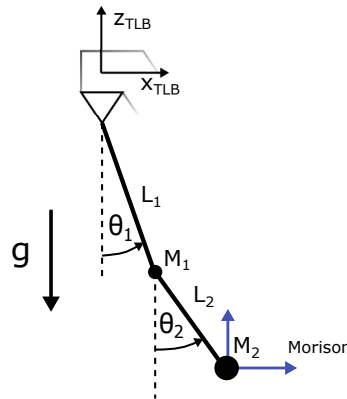


Figure 3.2: Double Pendulum model

The kinetic energy of the system is:

$$T = \frac{1}{2}M_1L_1^2\dot{\theta}_1^2 + \frac{1}{2}M_2(L_1^2\dot{\theta}_1^2 + L_2^2\dot{\theta}_2^2 + 2L_1L_2\theta_1\theta_2 \cos(\theta_2 - \theta_1)) \quad (3.15)$$

The potential energy of the system is:

$$V = M_1L_1g(1 - \cos\theta_1) + M_2g\{L_1(1 - \cos\theta_1) + L_2(1 - \cos\theta_2)\} \quad (3.16)$$

$$= g\{(M_1 + M_2)L_1(1 - \cos\theta_1) + M_2L_2(1 - \cos\theta_2)\} \quad (3.17)$$

The Lagrian of the system becomes:

$$L = T - V \quad (3.18)$$

$$= \frac{1}{2}M_1L_1^2\dot{\theta}_1^2 + \frac{1}{2}M_2(L_1^2\dot{\theta}_1^2 + L_2^2\dot{\theta}_2^2 + 2L_1L_2\theta_1\theta_2 \cos(\theta_2 - \theta_1)) - g\{(M_1 + M_2)L_1(1 - \cos\theta_1) + M_2L_2(1 - \cos\theta_2)\} \quad (3.19)$$

This equation of motion has to linearised assuming small angle approximation in order to conduct a frequency analysis:

$$\sin\theta \approx \theta \quad (3.20)$$

$$\cos\theta \approx 1 \quad (3.21)$$

In matrix form the equation of motion becomes:

$$\begin{bmatrix} (M_1 + M_2)L_1^2 & M_2L_1L_2 \\ M_2L_1L_2 & M_2L_2^2 \end{bmatrix} \begin{pmatrix} \ddot{\theta}_1 \\ \ddot{\theta}_2 \end{pmatrix} + \begin{bmatrix} (M_1 + M_2)L_1g & 0 \\ 0 & M_2L_2g \end{bmatrix} \begin{pmatrix} \theta_1 \\ \theta_2 \end{pmatrix} = \begin{pmatrix} 0 \\ 0 \end{pmatrix} \quad (3.22)$$

Which can be rewritten and shortened to:

$$\mathbf{M}\ddot{\theta} + \mathbf{K}\theta = 0 \quad (3.23)$$

$$\ddot{\theta} + \mathbf{M}^{-1}\mathbf{K}\theta = \ddot{\theta} + \mathbf{A}\theta = 0 \quad (3.24)$$

where

$$\mathbf{A} = \mathbf{M}^{-1}\mathbf{K} = \frac{1}{M_2L_2^2(M_1 + M_2)L_1^2 - (M_2L_1L_2)^2} \begin{bmatrix} M_2L_2^2 & -M_2L_1L_2 \\ -M_2L_1L_2 & (M_1 + M_2)L_1^2 \end{bmatrix} \begin{bmatrix} (M_1 + M_2)L_1g & 0 \\ 0 & M_2L_2g \end{bmatrix} \quad (3.25)$$

In the case of jacket attached to the TLB, the mass of the jacket is significantly larger than that of the hoisting block ($m_{jacket} \ll m_{hoistblock}$). According to Kwiatkowski [6], and increase of mass of the lower member of the pendulum has a reducing influence of the vibration amplitude.

3.2. Time Domain

The forces governing the jacket motions are expected to behave non-linear and non-continuous, due to the non-linear drag and impact phenomena, among others. Therefore, a frequency domain simulation is not sufficient, as that assumes a steady state form of the response. As a consequence, a direct time domain simulation (TD) is considered. All non-linearities can be included in this approach. In short, the differential equations following from Newton's second law are integrated in the time domain, using a proper numerical method. The advantage is that it is possible to incorporate all non-linearities in the equation of motion. However, all input time records must be given and generated provided, such a the incoming wave records. However, since the generated wave records is generated, one cannot be certain of its validity. Additionally, the obtained simulation time series must be post-processed. Interpreting the results is difficult, since a hypothetical input record is used and one can not be certain it is a valid input. How the post processing is done is elaborated later this chapter.

One of the most popular and effective numerical methods for a time domain simulation is the fourth-order Runge-Kutta (RK) method [7]. It will be used in this thesis. The RK method is a single step process to numerically solve an initial value problem of a ordinary differential equation in the form of equation 3.26.

$$\begin{aligned} y' &= f(t, y) \\ y(t_0) &= y_0 \end{aligned} \quad (3.26)$$

Equation 3.26 can be rewritten in its equivalent integral form:

$$y(t) = y_0 + \int_{t_0}^t f(t_n, y_n) dx \quad n = 0, 1, 2, \dots \quad (3.27)$$

In turn, since equation 3.27 is continuous and we are searching for a discrete solution, the equation is approximated by *Euler's equation* [8]:

$$y_{n+1} = y_n + f(t_n, y_n) \cdot \Delta t \quad y(t_0) = y_0 \quad (3.28)$$

Equation 3.28 is an ordinary differential equation, whilst the equation that has to be solved is a 2^{nd} order differential equation. In order to solve this system in the time domain, the 2^{nd} order differential equation is rewritten into a system of 2 ordinary differential equations, the *state-space representation*.

$$x_1 = \theta \quad (3.29)$$

$$x_2 = \dot{\theta} \quad (3.30)$$

$$\dot{x}_1 = \dot{\theta} = x_2 \quad (3.31)$$

$$\dot{x}_2 = \ddot{\theta} \quad (3.32)$$

Consequently, the fourth-order Runge-Kutta is used to solve the system, of which only the initial conditions are known: $\mathbf{x}_0 = [x_1(0) \ x_2(0)]^T = [0 \ 0]$. These *initial values* corresponds to the starting position.

In *state-space representation*, this becomes:

$$t_{n+1} = t_n + \Delta t \quad (3.33)$$

$$x_{1,n+1} = x_{1,n} + x_{2,n} \cdot \Delta t \quad (3.34)$$

$$x_{2,n+1} = x_{2,n} - \{\dot{x}_2\} \cdot \Delta t \quad (3.35)$$

In equation 3.35, the term $\{\dot{x}_2\}$ is the equation of motion of the 2^{nd} order differential equation as function of x_1 and x_2 .

The initial conditions for the time domain simulation can be manually set to values above ($\mathbf{x}_0 = [0 \ 0]$). However, by using a nonlinear equation solver, the equilibrium point of the equation of motion (in state-space configuration) can be iteratively determined:

$$F(\mathbf{x}_0) = \begin{bmatrix} 0 \\ 0 \end{bmatrix} \quad (3.36)$$

From this equilibrium point, a time record is created. The interpretation of a time domain simulation is done by using a statistical analysis, briefly described in chapter 3.2.3.

3.2.1. Single Pendulum

As explained in previous sections, if small angles can not be assumed, and/or the pendulum experiences non linear effect such as quadratic drag. The equation of motion of the single pendulum can be left in its non-linear state, and by moving all terms that do not have an 2^{nd} order derivative to the right hand side, the equation can be used in a time domain simulation. In that case, the equation becomes:

$$\ddot{\theta} = \frac{1}{-L(\cos(\theta))^2 m - L(\sin(\theta))^2 m} 2L \cos(\theta) \sin(\theta) m \dot{\theta}^2 + \sin(\theta) gm - F_{mor,x} \cos(\theta) - F_{mor,z} \sin(\theta) - \cos(\theta) ux(t) - \sin(\theta) uz(t) \quad (3.37)$$

where F_{mor} are the Morison force components. These are obtained by an instantaneous force integration over the structure. How this is done exactly will be explained later in this chapter.

$$F_{mor}(t) = \begin{bmatrix} F_{mor,x} \\ F_{mor,y} \\ F_{mor,z} \end{bmatrix} = \text{fn}(\theta, \dot{\theta}, \ddot{\theta}, t) \quad (3.38)$$

Since this function includes a second derivative in time in the right hand side of the equation, the rotational acceleration of the previous time step is used in the time domain solver (equation 3.39). It is assumed that this has a negligible influence for this thesis. However

$$F_{mor}(t_{n+1}) = \text{fn}(\theta_n, \dot{\theta}_n, \ddot{\theta}_{n-1}, t_n) \quad (3.39)$$

3.2.2. Double Pendulum

The equation of motion of the double pendulum in state space representation is quite more work to derive. Therefore, use is made of Maple, a symbolic computing package by MapleSoft. The equation of motion, without any form of linearisation, becomes:

$$\ddot{\theta}_1 = \frac{1}{-LI(\cos(\theta_1 - \theta_2))^2 m_2 + LI m_1 + L_1 m_2} \cdot [-L_1 \sin(\theta_1 - \theta_2) \cos(\theta_1 - \theta_2) m_2 \dot{\theta}_1^2 - L_2 \cos(\theta_1 - \theta_2) \sin(2\theta_2) m_2 \dot{\theta}_2^2 + L_2 \sin(\theta_1 + \theta_2) m_2 \dot{\theta}_2^2 + \cos(\theta_1 - \theta_2) \sin(\theta_2) g m_2 - F_{morx} \cos(\theta_2) \cos(\theta_1 - \theta_2) - F_{morz} \sin(\theta_2) \cos(\theta_1 - \theta_2) - \sin(\theta_1) g m_1 - \sin(\theta_1) g m_2 + F_{morx} \cos(\theta_1) + F_{morz} \sin(\theta_1) + \sin(\theta_1) ux(t) + \cos(\theta_1) ux(t)] \quad (3.40)$$

$$\ddot{\theta}_2 = \frac{1}{L_2^2 m_2 m_1 - L_2^2 (\cos(\theta_1 - \theta_2))^2 m_2^2 + L_2^2 m_2^2} [-L_2^2 \sin(\theta_1 + \theta_2) \cos(\theta_1 - \theta_2) m_2^2 \omega^2 + L_1 L_2 m_2 \dot{\theta}_1^2 \sin(\theta_1 - \theta_2) m_1 + L_1 L_2 m_2^2 \dot{\theta}_1^2 \sin(\theta_1 - \theta_2) + L_2^2 m_2 \dot{\theta}_2^2 \sin(2\theta_2) m_1 + L_2^2 m_2^2 \dot{\theta}_2^2 \sin(2\theta_2) + L_2 \sin(\theta_1) \cos(\theta_1 - \theta_2) g m_1 m_2 + L_2 \sin(\theta_1) \cos(\theta_1 - \theta_2) g m_2^2 - F_{morx} L_2 \cos(\theta_1) \cos(\theta_1 - \theta_2) m_2 - F_{morz} L_2 \sin(\theta_1) \cos(\theta_1 - \theta_2) m_2 - L_2 \sin(\theta_1) \cos(\theta_1 - \theta_2) m_2 ux(t) - L_2 \cos(\theta_1) \cos(\theta_1 - \theta_2) m_2 ux(t) - L_2 \sin(\theta_2) g m_2 m_1 - L_2 \sin(\theta_2) g m_2^2 + F_{morx} L_2 \cos(\theta_2) m_1 + F_{morx} L_2 \cos(\theta_2) m_2 + F_{morz} L_2 \sin(\theta_2) m_1 + F_{morz} L_2 \sin(\theta_2) m_2 - M(\cos(\theta_1 - \theta_2))^2 m_2 + M m_1 + M m_2] \quad (3.41)$$

In the equations of motions of the single and double pendulum, a time-dependent terms are present ($ux(t)$ and $uz(t)$). This follow from a pre obtained time record of the tip motion. More on this will be explained in chapter 3.4.

3.2.3. Time Domain Post-processing

To draw information conclusions from a time series, descriptive statistical analyses are conducted. After all, if the simulation includes random wave (phases), consecutive identical simulations will never be exactly the same due to this randomness, but also due to numerical discrepancies.

Responses from irregular sea states with a Gaussian distributed wave height in combination with narrow banded response spectrum, obey Rayleigh distributed [9] wave amplitudes ($R_a(\omega)$). Only short term predictions are considered. From an given or simulated time series, first the the standard deviation, σ , is calculated with equation 3.42. This standard deviation squared approximates the area underneath the response spectrum, also the 0th moment of response spectrum (equation 3.45 and 3.46).

$$\sigma = \sqrt{\frac{1}{N-1} \sum_{n=1}^N (R_a - \mu)^2} \quad (3.42)$$

$$\sigma^2 \approx m_{0R} \quad (3.43)$$

m_{0R} can be used in predicting what the significant amplitude, maximum amplitude and what the probability is the amplitude exceeds a certain value. Since the response obeys a Rayleigh distribution, the probability density function of equation 3.44 can be used.

$$f(R_a) = \frac{R_a}{\sigma_R^2} \cdot e^{-\frac{R_a^2}{2\sigma_R^2}} \quad (3.44)$$

where:

$$|H_{R\zeta}(\omega)| = \frac{R_a(\omega)}{S_\zeta(\omega)} \quad (3.45)$$

$$S_{R\zeta} = |H_{R\zeta}(\omega)|^2 \cdot S_\zeta(\omega) \quad (3.46)$$

The equation of the maximum motion is based on the statistical occurrence of once every 1000 oscillations, $f(R_a) = P\{R_a > R_{a,max}\} = \frac{1}{1000}$

$$r_{r1/3} = 2\sigma \quad (3.47)$$

$$x_{max} = 1.86 x_{1/3} \quad (3.48)$$

3.3. Morison forces

When considering vessel motions, it is assumed that the vessel is a large rigid body with respect to the incoming waves. However, to calculate the forces on a slender body, with members that are significantly smaller than the incoming waves, i.e. $\frac{d}{\lambda} < 0.1$ to 0.2 where d is the characteristic diameter of the structure and λ the wavelength, an other approach is used. In the derivation of these forces, it is assumed that the ambient fluid motions are not affected by the presence of the structure and that there are no diffracted waves [10]. In other words, the structure is 'transparent'.

Consistent with Newton's second law, forces result in acceleration. So there must be a force driving the acceleration of the fluid, caused by pressure gradient along an hypothetical cylinder. Now for such small member, a pressure integration is conducted along the surface. This results in an inertial force. From experiments, it is observed that there is also a force present that is related to the squared velocity at the member, a drag force.

This approach was first introduced by Morison [11]:

$$F_{morison}(t) = F_{Inertia} + F_{Drag} = \rho \frac{\pi}{4} C_M D^2 \cdot \dot{u}(t) + \frac{1}{2} \rho C_D \cdot u(t) |u(t)| \quad (3.49)$$

- $F(t)$ = excitation force [N]
- ρ = water density [kg/m^3]
- C_m = inertia coefficient (-)
- D = cylinder diameter [m]
- $\dot{u}(t)$ = particle flow acceleration (m/s^2)
- C_D = drag coefficient (-)
- $u(t)$ = particle flow velocity [m/s]

All members of the jacket are considered to be perfectly round shaped, therefore eliminating the effect of a lift force [12].

3.3.1. Morison force integration over a structure

A jacket consists of a finite number of members, N_m . When fixed to the seabed (i.e. it is unable to move wrt to the earth), with an regular incoming wave, the Morison forces, for example in X-direction, are calculated with equation 3.50. Here it is assumed that the drag and inertia coefficient and the diameter remain constant over the length.

$$dF = \frac{1}{2} \rho D C_D |u_f| u_f + \frac{\pi}{4} \rho D^2 C_M \dot{u}_f \quad (3.50)$$

The motions of the jacket included gives equation 3.51.

$$dF = \frac{1}{2}\rho DC_D |u_f - u_s| (u_f - u_s) + \frac{\pi}{4}\rho D^2 C_M \dot{u}_f - \frac{\pi}{4}\rho D^2 C_a \dot{u}_s \quad (3.51)$$

In equation 3.51, the subscript f and s denote the fluid and structure motions, respectively. The total force on the member is obtained by integrating over the length of the member, as can be seen in equation 3.52 - 3.54.

$$F_x = \int_{L_e}^{L_e+dL} \left\{ \frac{1}{2}\rho DC_D |\bar{u}_{fx} - \bar{u}_{sx}| (u_{fx} - u_{sx}) + \frac{\pi}{4}\rho C_M \dot{u}_{fx} - \frac{\pi}{4}\rho C_a \dot{u}_{sx} \right\} dx \quad (3.52)$$

$$F_y = \int_{L_e}^{L_e+dL} \left\{ \frac{1}{2}\rho DC_D |\bar{u}_{fy} - \bar{u}_{sy}| (u_{fy} - u_{sy}) + \frac{\pi}{4}\rho C_M \dot{u}_{fy} - \frac{\pi}{4}\rho C_a \dot{u}_{sy} \right\} dy \quad (3.53)$$

$$F_z = \int_{L_e}^{L_e+dL} \left\{ \frac{1}{2}\rho DC_D |\bar{u}_{fz} - \bar{u}_{sz}| (u_{fz} - u_{sz}) + \frac{\pi}{4}\rho C_M \dot{u}_{fz} - \frac{\pi}{4}\rho C_a \dot{u}_{sz} \right\} dz \quad (3.54)$$

where u_{fx} and \dot{u}_{fx} are the fluid velocity and acceleration, derived from potential flow [13] from the incoming wave respectively:

$$\Phi = \Phi_w \quad (3.55)$$

and than:

$$u_{fx} = \frac{\partial \Phi}{\partial x} = \zeta_a \omega \cdot e^{kz} \cos(kx - \omega t) + u_{x,current} \quad (3.56)$$

$$\dot{u}_{fx} = \frac{\partial \Phi}{\partial x} \frac{d}{dt} = \zeta_a \omega^2 e^{kz} \sin(kx - \omega t) \quad (3.57)$$

In equations 3.52 - 3.54, u_{sx} and \dot{u}_{sx} , represent the velocity and acceleration of the fluid wrt to the 'fixed' structure, which is equivalent the inverse of the motion of the structure wrt still water.

3.3.2. Wheeler stretching

The fluid velocity and wave height that is calculated above the mean water level should be extrapolated to the instantaneous change wave height. The most widely used is *Wheeler stretching*, as in figure 3.3. The holds that instead of extrapolating the exponential term (e^{kz}) to above mean water level, the vertical coordinate is stretched according to 3.58, where z_s is the original coordinate, η is the free surface elevation and d is the depth.

$$z = \frac{z_s - \eta}{1 + \eta/d} \quad (3.58)$$

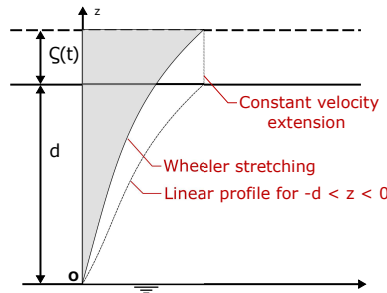


Figure 3.3: Wheeler stretching

Note that \bar{F} and \bar{u} , from equations 3.52 - 3.54, are the 6 DoF force and motion vectors of a single member. For a entire jacket, this force is summarized over the all the members (equation 3.59).

$$\bar{\mathbf{F}}_{jacket} = \sum_{n=1}^{N_m} \bar{\mathbf{F}}_{mor,n} \quad (3.59)$$

3.3.3. Vector calculations

To calculate the total forces and moments on a space truss such as jacket, each member is considered separately. The total force is obtained by integrating the force along its length. The jacket that is used for simulations is a stick figure (see figure 2.4). The nodes, or intersections between jacket members, are defined by their end points. The stick figure states that the external and internal forces exerted on the beams, act on the centroid of the member. The velocity and acceleration vectors are for most cases member not parallel or perpendicular to the jacket member, while only the velocity and acceleration component that is perpendicular to the jacket member causes a force.

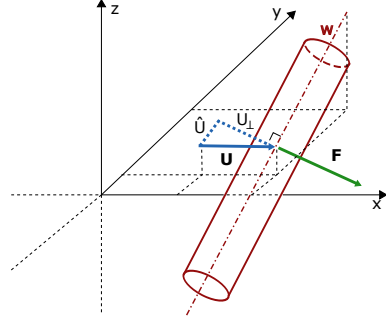


Figure 3.4: Vector representation of single jacket member

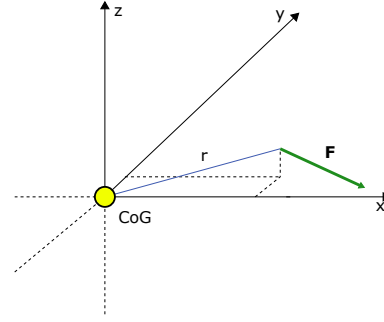


Figure 3.5: Resulting moment around CoG

The fluid kinematics, i.e. velocity and acceleration of the fluid in X,Y and Z direction can be calculated with potential wave theory [13], at every location at every instance (equation 3.56 and 3.57). According to Journée et al [13], the force, F_c , will act in the direction of U_p of course; this is perpendicular to the cylinder axis and in the plane defined by the cylinder axis and the approaching velocity vector, u' . So the jacket member will be considered as vector \bar{w} . The velocity component perpendicular to \bar{w} can be found by subtracting the orthogonal projection of the velocity on the jacket member vector \bar{w} from the velocity vector itself [14]:

$$u_{\perp} = u - \hat{u} \quad (3.60)$$

The orthogonal projection of the velocity on the jacket member w , \hat{u} , is found with:

$$\hat{u} = \frac{u \cdot n}{n \cdot n} n \quad (3.61)$$

where n is the unit vector parallel to w :

$$n = \frac{w}{|w|} \quad (3.62)$$

The above calculation also works for the acceleration. The force vector F can be calculated with u_{\perp} and \hat{u}_{\perp} with equations 3.52 - 3.53. This force vector then has a X, Y and Z component. For the total forces on the jacket, these the forces can be summarized from all separate jacket members. To obtain the moment on the jacket generated by the single jacket member, the cross product must be applied of the force F and the arm r from the CoG to the arm where the force is applied:

$$M_{CoG} = F \times r \quad (3.63)$$

3.4. Wave record generation

A time record for the tip motion should be provided. This will be generated using predetermined wave spectra. Based on the parameter given in the design load case of table 2.4, an incoming wave data can be generated, The wave height is based on airy wave theory [12]. Irregular random waves, such as a real sea state, is the summation of different frequency components of the wave spectrum.

$$\eta(t) = \sum_{n=1}^N A_k \cos k_n x - \omega_n t + \epsilon_n \quad (3.64)$$

As mentioned in chapter 2, a Pierson-Moskowitz spectrum will be used over JONSWAP spectrum. The curve of a PM spectrum is described in equation 3.65.

$$S_{PM}(\omega) = \frac{173 \cdot H_S^2}{T_1^4} \cdot \omega^{-5} \exp \left\{ -\frac{692}{T_1^4} \omega^{-4} \right\} \quad (3.65)$$

The spectrum is shown in graph 3.6 for a range of $0 \leq \omega < 2$ with a frequency step of $\Delta\omega = 0.0054$ [rad/s]. A time series constructed from this spectrum, with a constant frequency interval, would have repeating duration of 1200s, as calculated in equation 3.66.

$$D_{rep} = \frac{2\pi}{\Delta\omega} = 1200s \quad (3.66)$$

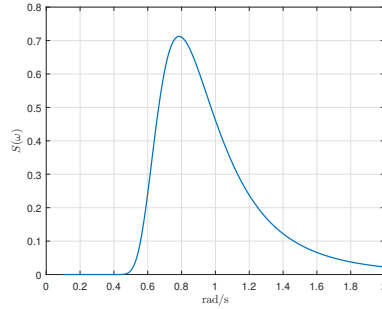


Figure 3.6: Pierson Moskowicz Spectrum

3.4.1. Phase lag

The motion of the two structures are excited by incoming waves. For both structures, the motions are translated to the motion of the CoG. However, since there is a distance between the two CoGs, there exist a phase lag between the exciting wave forces. In addition, this phase lag is different per wave frequency component for irregular waves.

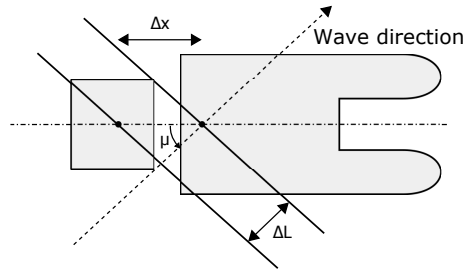


Figure 3.7: Phase lag difference

To calculate this lag $\Delta\epsilon(\omega)$, first the distance between the two CoG must be determined, and consequently the distance between two waves perpendicular to the wave direction with equation 3.67.

$$\Delta L = \Delta x \cdot \cos \mu \quad (3.67)$$

The phase lag is calculated with equation 3.68.

$$\epsilon_{pl} = k(\omega) \cdot \Delta L \quad (3.68)$$

where wave number k is found from the dispersion relation (equation 3.69). Since this equation is non-linear, it has to be solved iteratively.

$$\omega^2 = k \cdot g \cdot \tanh k \cdot h \quad (3.69)$$

The phase lag from the due to location of the jacket wrt the CoG of the vessel is substituted in equation 3.64, therefore obtain equation 3.70.

$$\eta(t) = \sum_{k=1}^N A_k \cos \omega_k t + \epsilon_k + \epsilon_{pl} \quad (3.70)$$

With equation 3.70 and the wave spectrum from equation 3.6, a time series of wave height at the CoG can be constructed. The phases ϵ_k are random at each frequency, for the interval $0 < \epsilon_k < 2\pi$. The amplitudes are calculated with equation 3.71. To maintain a consistent input during the simulation, the vector of random phases is generated once, and consequently kept constant. This gives the a wave height time series in figure 3.8.

$$A_k = \zeta_a = \sqrt{2 \cdot S_{\zeta(PM)}(\omega) \cdot \Delta\omega} \quad (3.71)$$

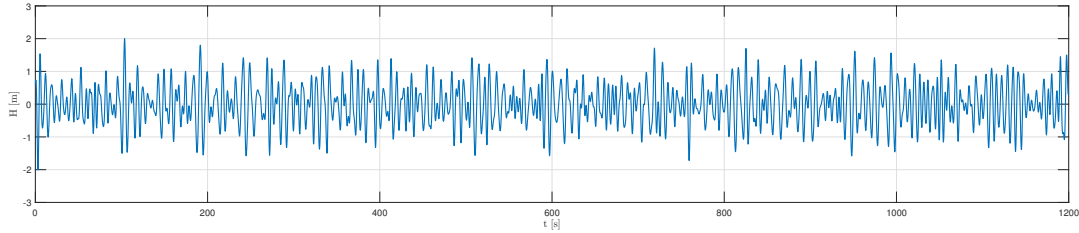


Figure 3.8: Time series wave height used for research

The motion of a floating vessel are described in 6 degrees of freedom; that is three translational (surge, sway, heave) and three rotational (roll, pitch, and yaw) DoFs. All these motions are relative to the vessel's centre of gravity. When the motions of and about the CoG are known, it is possible to determine the motion at any point P on the floating body. How the response of this theoretical point P is calculated below.

For a certain point $P(x_b, y_b, z_b)$ on the structure. For equation 3.37, the acceleration of the TLB tip is required. The angles of rotation are assumed to be small, therefore they can be linearised:

$$\sin(\phi) \approx \phi \quad (3.72)$$

$$\cos(\phi) \approx 1 \quad (3.73)$$

This gives the following translated motion of point P

$$x_p = x - y_b\psi + z_b\theta \quad (3.74)$$

$$y_p = y + x_b\psi - z_b\theta \quad (3.75)$$

$$z_p = z - x_b\theta + y_b\phi \quad (3.76)$$

3.5. Impact

Impact is the a primary cause of impulsive motions in structures, and they impose a sudden redistribution of momentum in the concerned bodies. It is a force applied for a short period, exciting the structures in all frequencies, being potentially harmful. Therefore, in marine environment, fenders are used to absorb the kinetic energy and reduce impact force on the structures by extending to time of contact and therefore the change in momentum. The common way to obtain design loads on structures and fendering systems is to estimate the amount of kinetic energy of the approaching structure [15].

$$p = \int_0^{t_c} F(t) dt \quad (3.77)$$

where

$$p = \text{normal impulse for compression} \quad (3.78)$$

$$F(t) = \text{compression or impact force} \quad (3.79)$$

$$t_c = \text{time at end of compression} \quad (3.80)$$

This can be simplified to:

$$p = mv \tag{3.81}$$

$$\Delta p = F\Delta t = m\Delta v \tag{3.82}$$

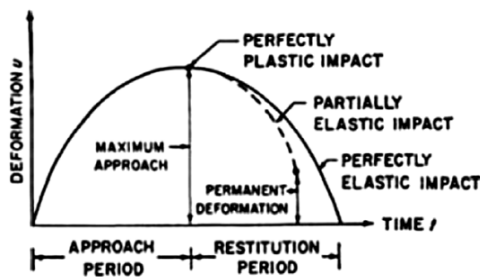
Where $F = F_{\text{average}}$ is the impact force and $F\Delta t$ the impulse, that equals the change in momentum (Δp). When the moving body has to be stopped by impact, the change in momentum is a fixed quantity. The impacting force, found with equation 3.82, can be decreased by extending the time of the collision, i.e. increasing Δt . A similar approach is to look at the work-energy relation:

$$Fs = \frac{1}{2}mv^2 \tag{3.83}$$

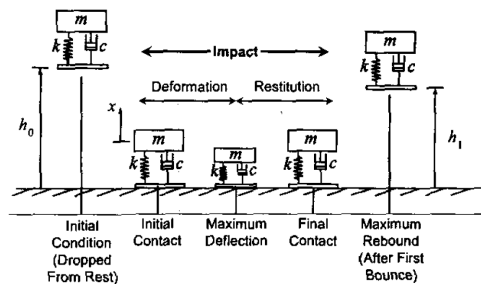
Where s is the distance travelled by the body in contact. By increasing the distance of collision, the impact force can be reduced.

Impact consist of three periods:

- **No contact.** Both structures are not in contact.
- **The approach period** Also called the compression phase. Its start is indicated with t_0 until t_c . Both structures are in contact. After the colliding bodies first touch, the contact forces rises and kinetic energy of relative motion is transformed into potential (elastic) energy.
- **The restitution period.** From t_c until t_f . The structures depart from each other. The elastic energy stored during compression generates the force that drives the bodies apart. If the impact is perfectly elastic, the restitution period and approach period at symmetrical.



(a) Classical impact process [16]



(b) Bouncing ball from [17]

Figure 3.9: Impact mechanisms

A sketch of the approach and restitution period can be seen in figure 3.9a. After contact, the normal component of the force F has an impulse p which equals the area under the curve in figure 3.9a, as in equation 3.77. According to Stronge [18], there is no way of obtaining the compression length, δ , directly without detailed information about the compliance of the colliding bodies. Therefore a numerical simulation is needed.

A possible measure for the amount of energy absorbed during the collision is to calculate the coefficient of restitution e_* . This is calculated with equation 3.84

$$e_* = \frac{p_f - p_c}{p_c} = \frac{v_f}{v_0} \tag{3.84}$$

Impact between multiple mechanical bodies is often modelled with a spring - damper system [19]. A similar phenomenon in marine industry, is the impact between fenders and vessels, or between a jetty and a ship during berthing [20]. How this impact is modelled, and than in particular the transition between contact and no contact is discussed in this chapter. In literature, multiple theories of this transition are used. According to A.Jönsson et al [19], a combination of the existing theories provides the most reliable outcome.

In impact mechanics, in particular the rigid body impact mechanics, there are two types of viscoelastic collision models, that describe the contact force arising from the compression of colliding bodies, the *Kelvin-Voight* and *Maxwell* model [18]. In figure 3.10 can be seen that both models consist of a damper and a spring, where the first is in series and the second is parallel. The Kelvin-Voight (left) will be used in this thesis.

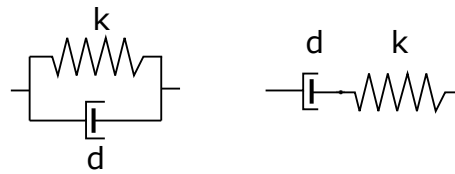


Figure 3.10: Impact of a body and fender

In mathematical terms:

$$F_c = \begin{cases} F_{fender} & \text{at contact} \\ 0 & \text{at no contact} \end{cases} \quad (3.85)$$

Where the force element is a linear elastic spring, parallel with a viscous damper. This gives:

$$F_{fender} = c(\dot{x}_{s1} - \dot{x}_{s2}) + k(x_{s1} - x_{s2}) \quad (3.86)$$

Here, $s1$ and $s2$ denote the two structures.

The transition between contact and non-contact is subjected to several implications. Two different transition conditions are considered, and a third ¹, which is a combination of the first two. The first condition is the relative distance (indicated with **A**). When considering only the distance between both structures is indicator between contact and no contact (i.e., $x_{s1} - x_{s2} = 0$ at impact), it fails to see true transition, because the relative velocity is larger than 0 (i.e., $\dot{x}_{s1} - \dot{x}_{s2} \neq 0$). The other option as indicator (**B**) used in literature [21] states that for both start and end of contact, the contact **force** is zero:

$$F_{fender} = 0 \quad (3.87)$$

This ensures that there will never be an adhesion force and that the contact force is continuous. However, in this transition, the relative velocity is larger than zero at every start of contact, which implies that there is force active before the distance is zero, which could influence the body dynamics.

A combination of the theories mentioned above will be used (**C**); at the start of every contact, the transition condition is dependent on the relative distance. At every transition from contact to non-contact, the contact force being equal to zero is the transition condition. In other terms:

$$\begin{aligned} x_{s1} - x_{s2} = 0 & \quad \text{contact to non-contact} \\ F_{fender} = 0 & \quad \text{non-contact to contact} \end{aligned} \quad (3.88)$$

3.6. Fenders

The offshore industry marine fenders are used to prevent large impacts. Marine fenders are equipment that come in a large variety of shapes, materials and working principle. Their task is to prevent vessels from colliding with jetties, structures or other ships. They do so by absorbing the kinetic energy in combination with a low reaction force so that the colliding structures are not damaged. The berthing of a vessel is a complex phenomenon, as the forces on the fender are affected by many factors [22], such as location of impact, geometry and rigidity of the ship, mechanical properties of the fenders, speed and angle of approach and environmental actions such as waves, wind and current.

For ship to ship operations, usually pneumatic fenders (figure 3.11) are used, due to the property that it has a low reaction force for a low deflection. They have an excellent energy absorption and load deflection. Therefore, characteristics of such fenders are used to model the interface between the jacket and PS

¹In the research mentioned above [19], there is another transition condition. It is based on condition C, but it also takes into account the phenomenon of the relaxation of the spring/damper. However, this phenomenon is neglected as it is expected that impact frequency is low enough for the spring-damper system to recover



Figure 3.11: Yokohoma pneumatic fender

Some typical characteristics can be seen in appendix B. From these figures, a typical fender stiffness of is extracted that will be used.

4

Model Design

This chapter describes how the models used for the JLS are built up. Relevant assumptions and calculations are described in subsequent sections.

4.1. MatLab model

The system is modelled in the 2D X-Z plane. A sketch of the system can be seen in figure 4.1. Two bodies can be identified, the vessel and the jacket. The vessel consists of the hull and the tilting lift beam, rigidly connected to the hull. The jacket is connected at the top of the TLB with hoisting cables, so that it pivots around the TLB tip. Both the vessel and the jacket are initially for this research restricted to move in only the X-Z plane, so that the Y direction (surge and roll and yaw) is locked. Both models are subjected to an incoming wave at $\mu = 0$ because it is expected that the jacket motion relative to the PS will show the largest fluctuations.

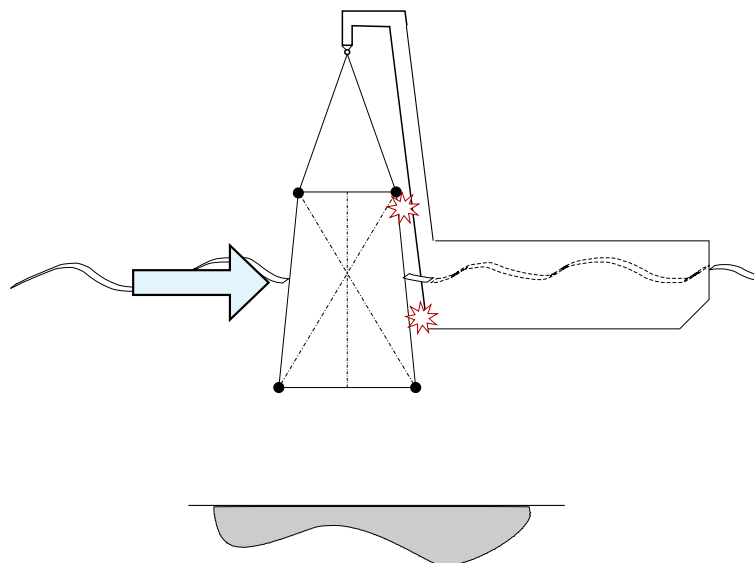


Figure 4.1: Simplified sketch of model

Two models of the suspended jacket will be modelled. The first will be considered as a swinging pendulum, whose pivot point is subjected to the imposed motion of the vessel. The a simplified representation can be seen in figure 4.1. Important assumptions that will be elaborated in this chapter are:

- The motion of the jacket does not significantly influence the motion of the vessel. Therefore, the motion imposed motion of the TLB can be calculated independently in advance.
- The hoisting cable configuration can be modelled as an inextensible rod

The assumptions will be more elaborated in this chapter. In table 4.1 the dimensions of both pendulum models are given.

Double Pendulum			Single Pendulum		
Dimension		Description	Dimension		Description
L1	67.5	Length hoisting cables [m]	L	154.5	Length tip to jacket CoG [m]
L2	87	Length top jacket - CoG [m]	M	14055	Total mass [tonnes]
M1	107	Mass hoisting wires [tonnes]			
M2	13948	Mass jacket [tonnes]			

Table 4.1: Pendulum dimensions

When the values from table 4.1 are substituted in matrix **A** from the double pendulum (equation 3.25), this becomes:

$$A = \begin{bmatrix} 19.090 & -18.945 \\ -14.811 & 24.605 \end{bmatrix} \quad (4.1)$$

The eigenvalues, or undamped natural frequencies, are calculated of this system with the values from table 4.1

$$\lambda_1 = 4.871 \text{ rad/s} \quad (4.2)$$

$$\lambda_2 = 38.82 \text{ rad/s} \quad (4.3)$$

$$(4.4)$$

The corresponding mode shapes are:

$$\begin{pmatrix} \theta_1 \\ \theta_2 \end{pmatrix}_{\lambda=\lambda_1} = \frac{1}{4.871} = 0.2053 \quad (4.5)$$

and

$$\begin{pmatrix} \theta_1 \\ \theta_2 \end{pmatrix}_{\lambda=\lambda_2} = \frac{1}{38.82} = 0.0258 \quad (4.6)$$

4.1.1. Vessel Motion

To investigate the effect of the jacket furthermore, first the Response Amplitude Operators are computed with Ansys AQWA. The resulting RAOs can be found in figure 4.6. For more details on the Ansys AQWA model, see chapter 4.1.1.

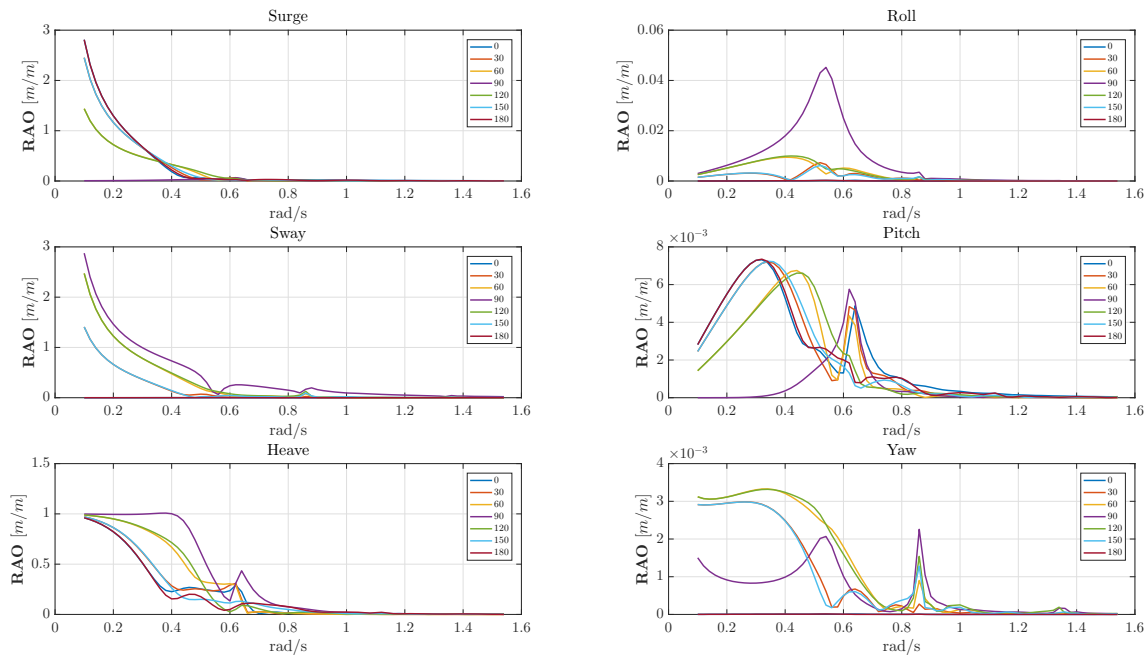


Figure 4.2: Response Amplitude Operator of the PS

As mentioned in chapter 3, motion of the pivot point of the pendulum models equals the motion of the TLB tip. When equation 3.74 is applied on the wave train from figure 3.8, this results in the heave motion of figure 4.3 and 4.4 for load case 2 (table 2.5) for 200 seconds.

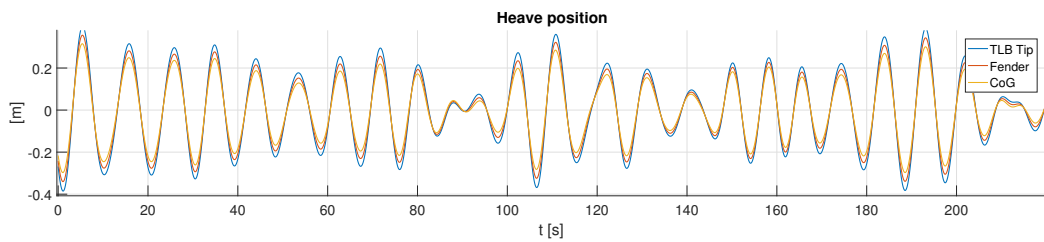


Figure 4.3: Heave motion of different positions

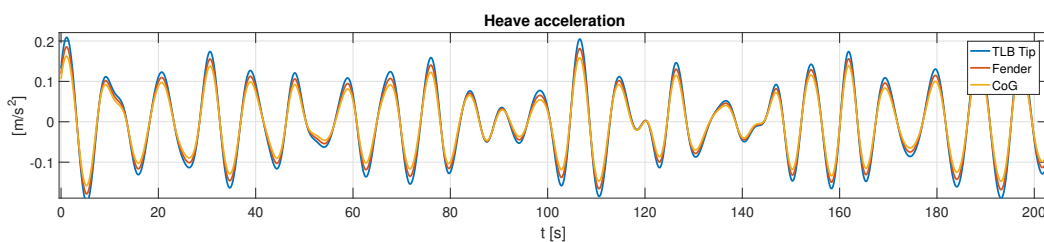


Figure 4.4: Heave acceleration of different positions

4.1.2. Motion influences of jacket

When the jacket is attached to the TLB, and suspended from the tip, the vessel motions will be influenced by the jacket motions. However, the question is whether these motions are significant. Though this question could be a research on itself, a preliminary check is conducted to estimate the effect, namely by the comparison of structures' masses.

For different operational modes of the PS, the ballasting is adjusted and therewith the draft. So for the mentioned calculation, the weight from the PS is at a draft of 17 meters. This is less draft for actual JLS operation. However, this has a positive effect on the result, since the ratio would increase for a larger draft (and thus larger mass). The ratio is calculated to be 2.1%.

$$r = \frac{m_{\text{jacket}}}{m_{\text{vessel}}} = \frac{14.000 \text{ tonnes}}{682.100 \text{ tonnes}} \approx 2.1\% \quad (4.7)$$

To provide additional insight into the effect of the jacket on the vessel motions, two point masses are added at the end of both TLB tips, rigidly connected to tip of the TLBs. Both masses have a magnitude of $7 \cdot 10^7 \text{ kg}$. Together they are equal to the submerged weight of the jacket. During the jacket lifting, the vessel is ballasted to even the keel trim. Thus, in order to maintain a moment equilibrium around the Y-axis in the model, another point mass is added (see figure 4.2), which is calculated with equation 4.8 to be equal to $4.86 \cdot 10^6 \text{ kg}$.

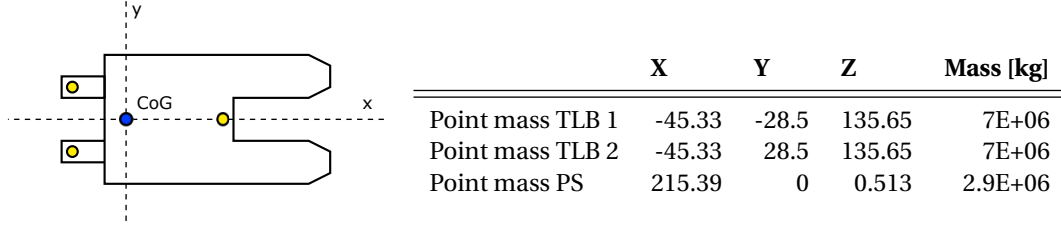


Table 4.2: Point mass locations

$$2 \cdot m_{p,TLB} \cdot r_{x,CoG-TLB} = m_{p,PS} \cdot r_{x,CoG-X_{m_p}} \quad (4.8)$$

The new equivalent RAOs are calculated of the vessel, and consequently for each DoF and each frequency, the equivalent RAO's is subtracted from the other (equation 4.9)

$$\delta_{RAO}(\omega, i) = RAO_i(\omega) - RAO_{i,eq}(\omega) \quad \text{for } i = 1 - 6 \quad (4.9)$$

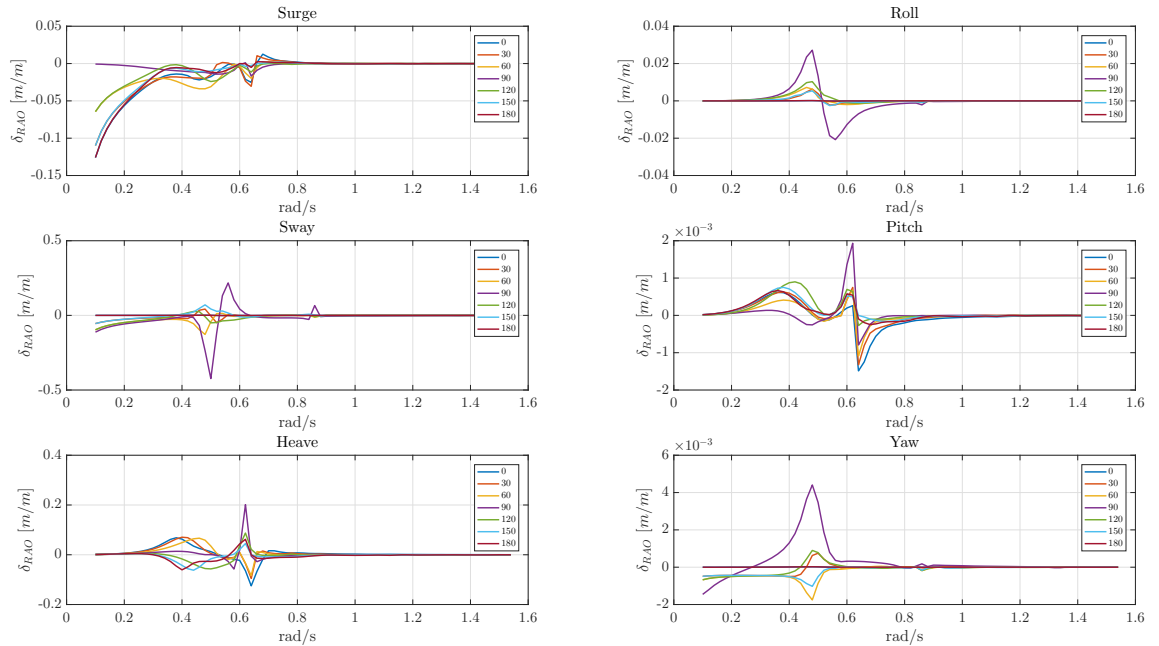


Figure 4.6: Difference RAOs of the PS

When compared to the RAOs in figure 4.6, it can be observed that these point masses do not have a large influence on the RAOs, especially for an incoming wave of $\mu = 0$. Therefore, it is assumed that the motion of the suspension point can be imposed with a previous generated motion time series.

4.1.3. Cable properties

In the equation of motion 3.37, the rod is assumed to be inextensible. In reality, the hoisting configuration has a certain stiffness. All of the wires, sheaving, hoisting length can be combined to a equivalent wire stiffness.

To determine whether the assumption of the inextensible rod is valid, the system is compared to a simple mass- spring system of figure 4.7. The stiffness is equal to twice the equivalent stiffness of the main hoist system (since it is connected to two beams), which is calculated to be $7.7 \cdot 10^7 \frac{N}{m}$ [2]. The weight of the jacket is the submerged weight. The natural frequency is calculated in equation 4.10. It should be noted that though the system is preloaded, this does not affect the natural frequency [7]. This value is significantly higher than the frequency of incoming waves. Therefore, the effect of the extensibility of the cable is neglected in the equation of motion.

$$\omega_n = \sqrt{\frac{k_{eq}}{m_{submerged}}} \approx \sqrt{\frac{7.7 \cdot 10^7}{1.4 \cdot 10^7}} = 2.3 \text{ rad/s} \quad (4.10)$$

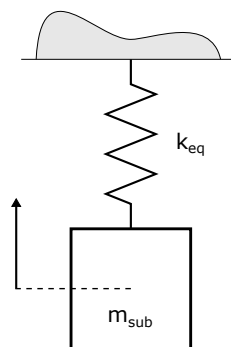


Figure 4.7: Mass Spring system

4.1.4. Inertia coefficient

In equation 3.49 there are two yet unknown constants C_M and C_D , the inertia and drag coefficient respectively. By theoretical derivation, C_M is equal to 2 [13], as it takes into account two, in theory equal, phenomena; the Froude Krilov force due to the undisturbed flow at the cylinder wall location, and the force due to the disturbance of the flow. However, by experimenting, it is found that the force due to the disturbance of the flow, is less than 1. This difference is taken into account by means of a the coefficient C_a , the 'added mass' coefficient.

So, the inertia coefficient is defined as:

$$C_M = 1 + C_a \quad (4.11)$$

Where $0 < C_a < 1$ For small structure members, this value is usually assumed to be $C_a = 0.2$ (DNV standard RP-C205, article 6.9.1.3). This results in a total inertia coefficient of:

$$C_M = 1.2 \quad (4.12)$$

4.1.5. Drag coefficient

For normal flow, the drag coefficient C_D depends on the Reynolds number, the structure's roughness with respect to the diameter (Δ) and the fluid viscosity. As the drag force will be expressed in terms of a relative velocity, a single drag coefficient will be sufficient for all cylinders [12]. This value is obtained with figure 4.8

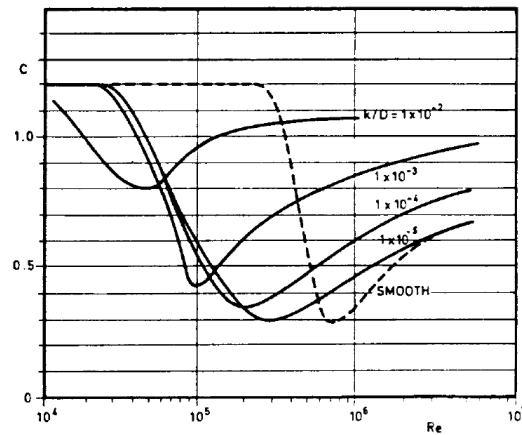


Figure 4.8: Drag coefficient [12]

The roughness is obtained with equation 4.13

$$\Delta = \frac{k}{D} \quad (4.13)$$

k is the roughness height, which is averaged from the known data for members covered in marine growth [12], is equal to $1 \cdot 10^{-2}$ and the average diameter of the jacket is 0.925 m

The Reynolds number, a dimensionless ratio between the inertial and viscous forces in a flow, is calculated with equation 4.14

$$Re = \frac{UD}{\nu} \quad (4.14)$$

Where:

U = mean fluid velocity [m/s]

D = average diameter [m]

ν = kinematic viscosity fluid [m^2/s]

The kinematic viscosity of seawater is $1.35 \cdot 10^{-6}$ at a temperature of $10^\circ C$ [12]. The mean fluid velocity needs to be estimated. The current velocity, as presented in table 2.4, is 0.5 m/s, is added with a contribution of wave velocity. At the free surface, this orbital velocity is $U_{fs,orbital} = \zeta_a \omega = 1.3m/s$. Due to the decay of this velocity with depth, the average wave velocity is estimated as $\frac{2}{3} U_{fs,orbital}$, which is $U = 0.5 + 0.87 = 1.3m/s$. This gives:

$$\Delta = 0.1081$$

$$Re = 8.9 \cdot 10^5$$

From figure 4.14 the drag coefficient can be estimated:

$$C_D \approx 1.08 \quad (4.15)$$

4.1.6. Inertia and drag dominance

The Morison equation is applicable on members with a diameter to wavelength ratio that is smaller $\frac{D}{\lambda} < 0.2$. When this condition is met, the ratio between drag and inertia forces can be estimated with the Keulegan-Carpenter number [23]:

$$KC = \frac{u_a T}{D} = 2\pi \frac{x_a}{D} \quad (4.16)$$

From Journée et al [13], several regions can be distinguished:

- **Inertia dominance** ($KC < 3$)

- **Linearized drag** Conservative, cross term in neglected ($3 < KC < 15$)
- **Full Morison equation** ($15 < KC < 45$)
- **Drag dominance** ($KC > 45$)

4.2. Jacket representation

The jacket described in chapter 2 consist of 572 different members (table 2.4). During a time domain simulation, for each member the force is calculated 3 times, namely due to its own motions, due to the environmental forces, and the due to the cross product (in case of drag (chapter 3.2.2.)). This force consists of drag and inertia. To summarize, at each time step approximately $572 \times 3 \times 2 \approx 3432$ computations are done. Especially during fast varying motions, when the variable time step is made small for the ODE solver, the simulation requires much computational effort. Therefore in this chapter, approaches are considered to decrease computational effort and increase simulation speed, without losing essential accuracy.

To compare the following approaches with each other, a force profile of the jacket is computed as can be seen in figure 4.9.

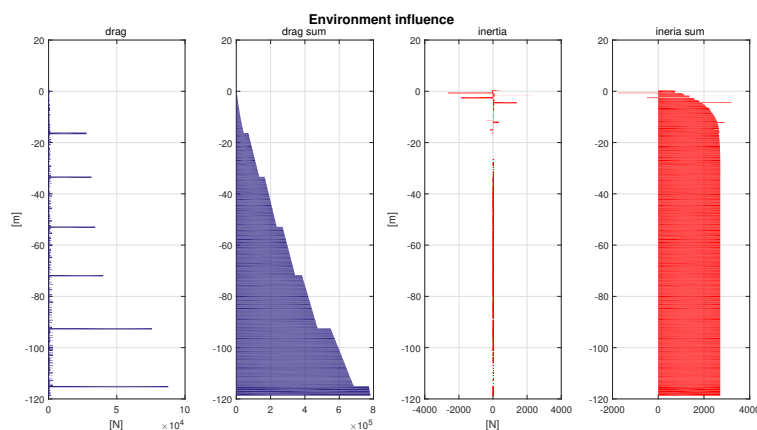


Figure 4.9: Force profile on jacket

- The blue graphs represent the drag force and the red graphs the inertial forces per meter depth. The left blue and red graph is the force at that specific depth. The right blue and red figure is the integral of the force per meter depth, starting from the top of the jacket downwards (referred to as sum plot). From these sum plot, it can be seen that the total drag force increases per meter depth, which is due to the uniform current applied on the jacket. The inertial forces stay constant after a certain depth, due to the exponential decay of the fluid accelerations.
- The total drag force in for this case is $F_{drag} \approx 0.75$ kN and $F_{inertia} \approx 2700$ N for $H_s = 2.5$ m, $u_{current} = 0.5$ m/s and $T_z = 5.7$

4.2.1. Equivalent Stick Model

The first approach to decrease computational power is to use the equivalent stick-model developed by Dubbers et al [24]. A graphical representation can be found in figure 4.10. Different stick ranges (R) are defined wrt to the SWL. For each of these stick ranges, an equivalent drag ($D_{de}(R)$) and inertia diameter ($D_{ie}(R)$) is calculated. This is done as follows: (from [24])

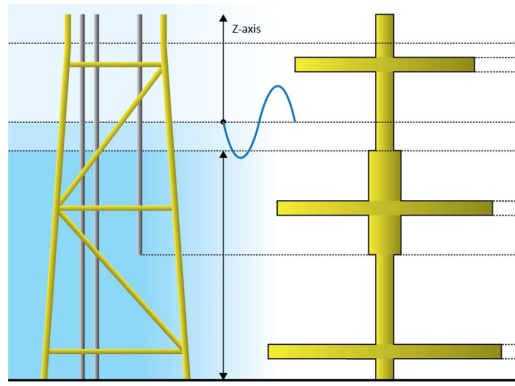


Figure 4.10: Graphical representation of equivalent stick-model method [24]

1. For each single member, the Δx , Δy and Δz are defined, and to which boundary it contributes, and what height of this range is ($E_0 = z_u - z_l$).
2. The following interim values are calculated:

$$p = \Delta y^2 + \Delta z^2 \quad (4.17)$$

$$L_{ij} = \sqrt{\Delta x^2 + p} \quad (4.18)$$

$$q = \frac{pD}{L_{ij}E_0} \quad (4.19)$$

3. The equivalent drag and inertia diameter is then calculated:

$$D_{de} = q \frac{\sqrt{p}}{L_{ij}} \quad (4.20)$$

$$D_{ie}^2 = qD \quad (4.21)$$

4. Finally, this calculation is repeated for each member, where the new equivalent diameter is added to the the value of the considered equivalent diameter per range

When the same regular wave as in 4.9 is applied on the equivalent stick model, the force profile of figure 4.11 is obtained for $t = 0$.

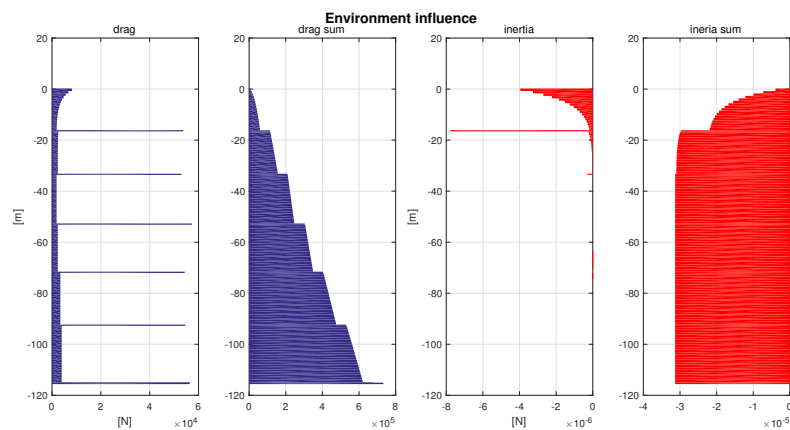


Figure 4.11: Force profile on equivalent jacket

- The drag force shows the same profile. The total drag is almost equal to the drag of the fully defined jacket model. However, the inertia deviates from the original model. This is attributed to the fact that there is no spacial variation in the equivalent stick model, while that variation is present in the original

model. In other words, due to the fact that the new model is located with a constant x and y coordinate, the inertia force at each member (or range) is in the same direction. In the original model, inertial force could cancel each other out due to their spacing relative to each other.

- The drag is dominant for the total force on the jacket. The inertial force deviate from the original model, however, these force are not significant.

4.2.2. Equivalent Cylinder

To run multiple simulations, the equivalent stick model showed be still requires much computational effort. Therefore, the equivalent stick-model is simplified to one single cylinder, with a equivalent drag and inertia diameter. The equivalent diameters are than scaled until the total force on the cylinder equals that of the fully defined jacket. That is with $D_{de} = 23$ m and $D_{ie} = 3.2$ m.

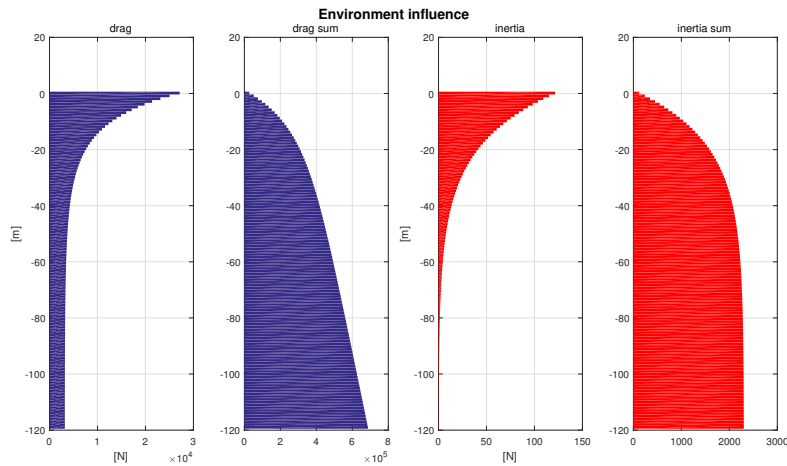


Figure 4.12: Force profile on single cylinder representation of jacket

4.3. AQWA model

Simultaneously with the pendulum approach, a model is developed in AQWA. For the first stages of the simulation AQWA-LINE is used. AQWA-LINE is the 3-D diffraction and radiation analysis program for wave force and structure response calculations, and can also be used for hydrostatic analysis. It performs analyses in the frequency domain and it assumes an ideal fluid, irrotational and incompressible.

A mesh of the PS is generated at a draft of 17 m (figure 4.14) and of the jacket (figure 4.13). A jacket model that was available has been scaled down to match the properties of the design jacket described in chapter 2.

The mesh of the PS consists of 4201 diffracting panels below sea level and 789 non-diffracting elements above sea level, whilst the jacket consists of 573 Morison tube elements. The draft of the vessel is 17 m. The vessel has a displacement of $\Delta = 5.32 \cdot 10^5$ m.

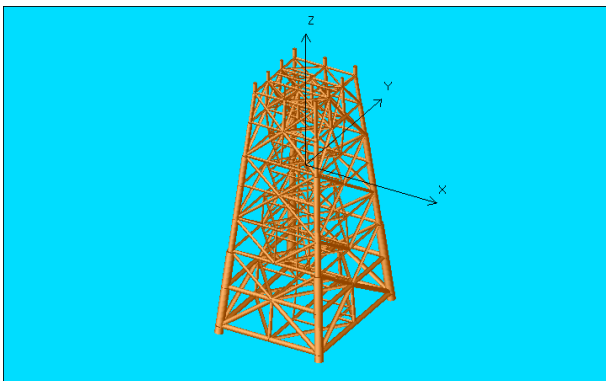


Figure 4.13: AQWA Model of jacket

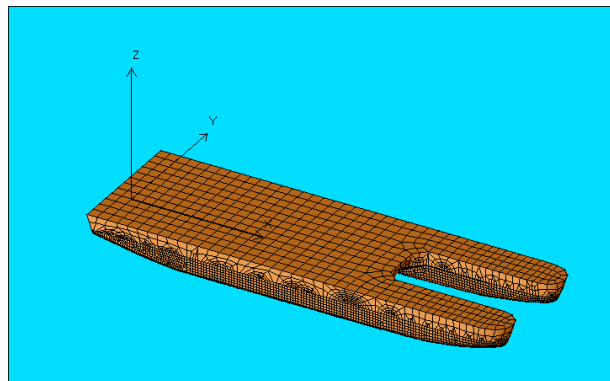


Figure 4.14: AQWA Model of PS

The frequency domain analysis gives the mass and spring matrices from the equation 4.23 - 4.26. The response of the structures in waves is calculated by solving the equation of motion in the frequency domain:

$$[\omega^2(M_s + A_s(\omega) - i\omega B(\omega) + C)]X(\omega) = F(\omega) \quad (4.22)$$

where:

M_s = Mass of structure [kg]

$A_s(\omega)$ = Added mass [kg]

C_s = Hydrostatic stiffness [N/m]

$B_s(\omega)$ = Damping [N/(m/s)]

$F(\omega)$ = Wave force (incident and diffracting) [N/m]

The added mass and damping are frequency dependent. Ansys AQWA solves these matrices for the PS and the jacket for a predefined frequency range of $0.1 < \omega < 1.7$ with a frequency step of $\omega_{step} = 0.02$ rad/s. Since the added mass and damping are frequency dependent (so they're matrices of $[6 \times 6 \times 68]$)

$$M_{vessel} = \begin{bmatrix} 5.28E+08 & 0 & 0 & 0 & 0 & 0 \\ 0 & 5.28E+08 & 0 & 0 & 0 & 0 \\ 0 & 0 & 5.28E+08 & 0 & 0 & 0 \\ 0 & 0 & 0 & 7.20E+11 & 2.38E+10 & 1.61E+11 \\ 0 & 0 & 0 & 2.38E+10 & 4.67E+12 & 4.60E+09 \\ 0 & 0 & 0 & 1.61E+11 & 4.60E+09 & 5.23E+12 \end{bmatrix} \quad (4.23)$$

$$M_{jacket} = \begin{bmatrix} 1.40E+07 & 0 & 0 & 0 & 0 & 0 \\ 0 & 1.40E+07 & 0 & 0 & 0 & 0 \\ 0 & 0 & 1.40E+07 & 0 & 0 & 0 \\ 0 & 0 & 0 & 3.65E+10 & 4.22E+08 & 6.49E+08 \\ 0 & 0 & 0 & 4.22E+08 & 3.30E+10 & 7.90E+08 \\ 0 & 0 & 0 & 6.49E+08 & 7.90E+08 & 1.69E+10 \end{bmatrix} \quad (4.24)$$

$$C_{vessel} = \begin{bmatrix} 0 & 0 & 0 & 0 & 0 & 0 \\ 0 & 0 & 0 & 0 & 0 & 0 \\ 0 & 0 & 3.68E+08 & -3.98E+03 & 3.54E+09 & 0 \\ 0 & 0 & -3.98E+03 & 4.51E+11 & -1.66E+05 & 3.47E+10 \\ 0 & 0 & 3.54E+09 & -1.66E+05 & 3.63E+12 & 1.47E+05 \\ 0 & 0 & 0 & 0 & 0 & 0 \end{bmatrix} \quad (4.25)$$

$$C_{jacket} = \begin{bmatrix} 0 & 0 & 0 & 0 & 0 & 0 \\ 0 & 0 & 0 & 0 & 0 & 0 \\ 0 & 0 & 1.02E+04 & -8.31E+04 & -5.60E+04 & 0.00E+00 \\ 0 & 0 & -8.31E+04 & 1.36E+07 & -2.46E+06 & -1.58E+04 \\ 0 & 0 & -5.60E+04 & -2.46E+06 & 8.65E+06 & 2.20E+04 \\ 0 & 0 & 0 & 0 & 0 & 0 \end{bmatrix} \quad (4.26)$$

With the results from the AQWA frequency domain analysis, also the RAOs from figure 4.6 are computed.

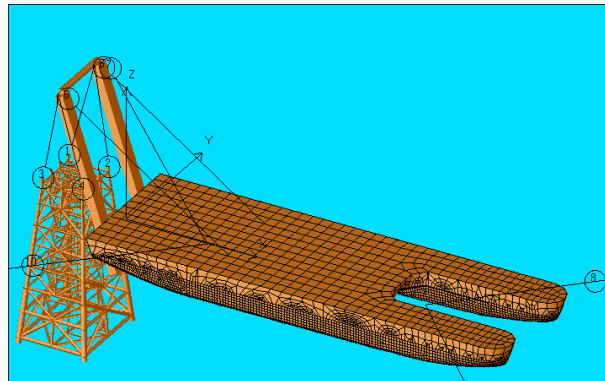


Figure 4.15: AQWA model PS with Forties C Jacket

In AQWA, the two structures can be coupled into one model for AQWA-DRIFT. This is the time domain program for drift frequency and wave frequency structure analysis in irregular waves.

Prior to the tilting phase, the jacket is lifted and tilted, in such a way that the slope of the jacket matches the initial slope of the TLBS. It does so by varying the aft and front hoisting wires on the jacket. This initial rotation has an influence on which fender will make contact first.

In AQWA, fenders are added in between the locations of the support structures (or grillages), and the joints on the jacket corresponding to the grillage locations. The axial force in a fender is determined with: The location of the fenders is given in table 4.3

Location measuring points			
	X	Y	Z
Upper support structure (A)	-24.7	0	55.81
Lower support structure (B)	-6.845	0	-18

Table 4.3: Measuring locations

The stiffness is given in equation 4.27

$$F_c = \begin{cases} k_1 \Delta L + k_2 (\Delta L)^2 + k_3 (\Delta L)^3 + k_4 (\Delta L)^4 + k_5 (\Delta L)^5 & \text{if } \Delta L > 0 \\ 0 & \text{if } \Delta L \leq 0 \end{cases} \quad (4.27)$$

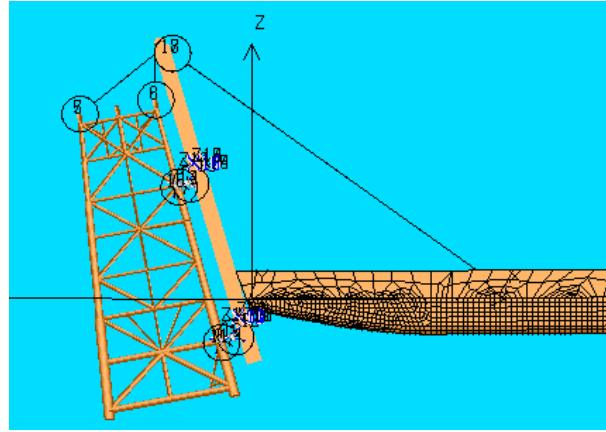


Figure 4.16: AQWA model PS with rotated jacket from side

4.3.1. Relative vs. Absolute Velocity approach in Frequency domain approach

The Morison force on the jacket is highly non-linear. In frequency domain analysis of the jacket, there are several terms that need attention. The term $|u_f - u_s|(u_f - u_s)$ in equation 3.50 can be worked out to $u_f^2 + u_s^2 - 2u_f u_s$. The first and second component, the external fluid force component and the internal motion force component respectively, can be split in the equation of motion. But especially the third component of this equation adds extra difficulties to find a solution. Two options are presented to overcome this problem:

- **Conservative approach.** Neglect the term $-2u_f u_s$. Due to negative term, the contribution of this term has a decreasing effect on the total force. A very conservative approach would be to leave out this term. The structures' response would be higher
- **Drag linearisation.** In equation 3.50, the term $|u_f - u_s|$ can be replaced by a factor multiplied by the root mean square of the relative velocity. According to Borgman [25], this factor is

$$\alpha = \sqrt{\frac{8}{\pi}} \quad (4.28)$$

This gives:

$$\begin{aligned} dF_{drag} &= \frac{1}{2} \rho D C_D \alpha u_{rms} (u_f - u_s) \\ &= \frac{1}{2} \rho D C_D \alpha u_{rms} u_f - \frac{1}{2} \rho D C_D \alpha u_{rms} u_s \end{aligned} \quad (4.29)$$

5

Simulation results

In this chapter, the results from the simulations with the different models are presented, provided with comments, observations and conclusions.

In chapter 2, table 2.5, several different load cases are defined in accordance with the operability of different operation modes of the PS. For convenience, this table is repeated below.

Load case	Based on operational limit of	H_s [m]	T_z [s]	Current velocity u_c [m/s]	Spectrum
1	Transfer	1	4.5	0.5	PM
2	Installation	2.5	5.7	0.5	PM
3	Transport (no heading control)	6	8.5	0.5	PM
4	Transport (w heading control)	10	10	0.5	PM

Table 5.1: Environmental load cases

5.1. Structure motions

The first part of the simulations chapter is to compare the motions of the structure, prior to the moment of impact. A time domain simulation with the self developed pendulum model is conducted, in combination with the AQWA model. The environmental conditions that will be discussed are described in 2.5, load case 2. Additional sensitivity analysis with varying loadcases and other parameters. Additional motion time series can be found in the appendix.

From the obtained time series, statistical analysis is conducted for Rayleigh distributed amplitudes, as presented and briefly explained in chapter 3. Four different aspects of these time series are compared:

- The horizontal and vertical position (in m) of the suspension point in both pendulums, representing the tip of the TLBs. These are calculated with the RAOs and incoming wave spectrum.
- The horizontal and vertical position (in m) of the mass of the single pendulum, the position of the lower mass of the double pendulum and the CoG of the jacket wrt to its equilibrium point.
- The tension (in N) in the rod and the hoisting wires.
- The momentum (in kg m/s) of the jacket in X and Z direction. This is calculated with equation 3.81

The results from the time domain simulation of the single and double pendulum and AQWA model for design load case 2 are given in figure 6.7 , 6.8 and 5.3, respectively.

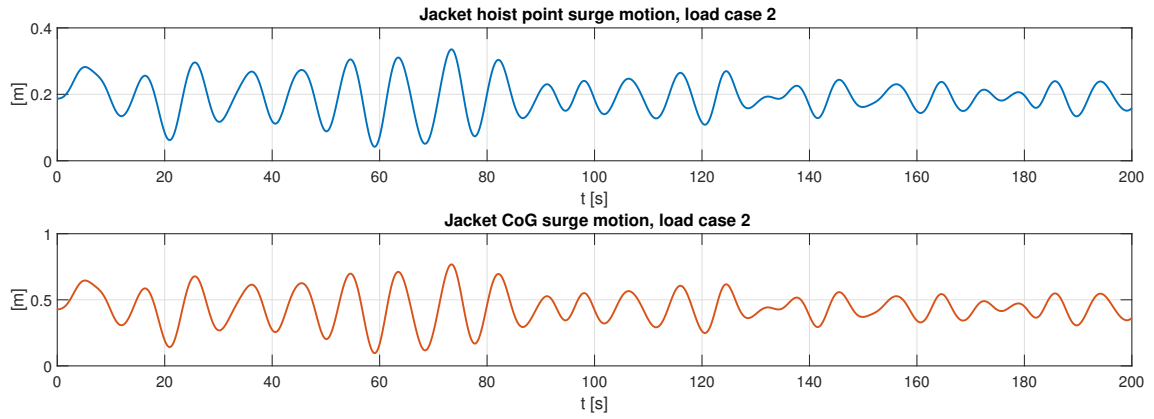


Figure 5.1: Surge motion load case 2, single pendulum

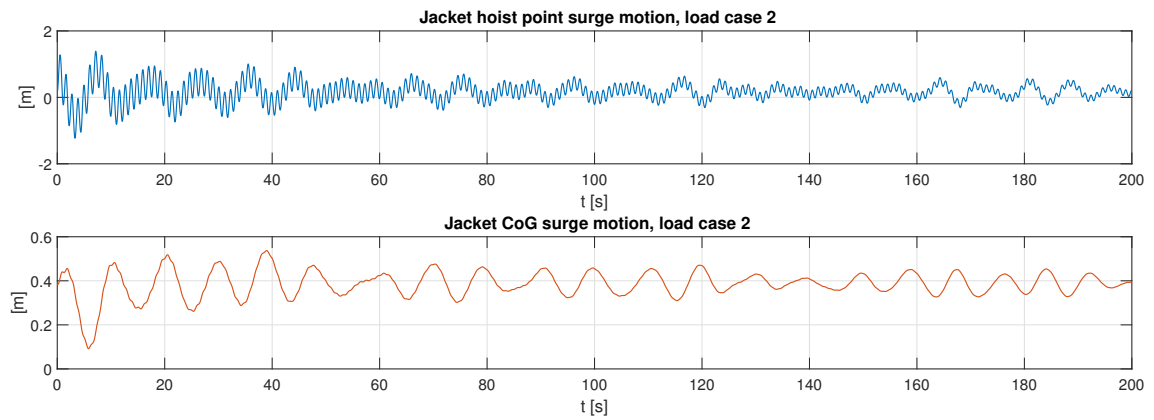


Figure 5.2: Surge motion load case 2, double pendulum

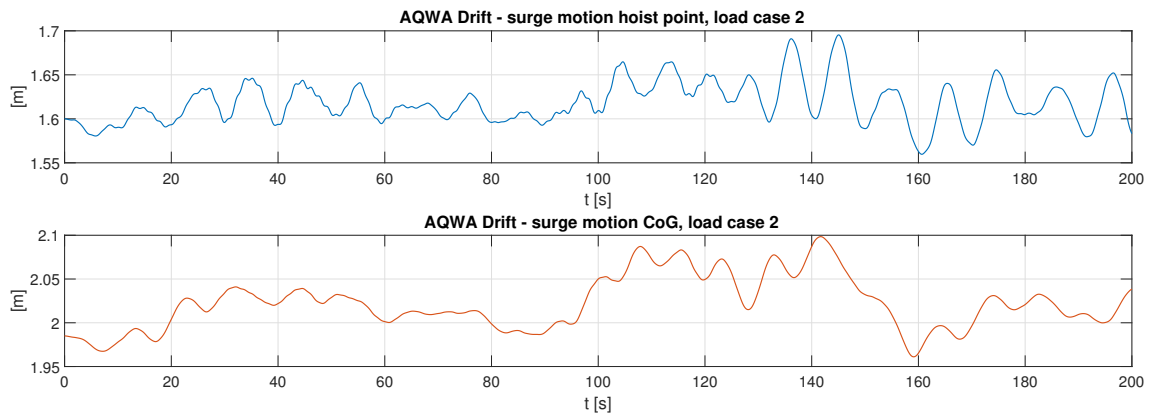


Figure 5.3: AQWA Simulation Surge motion load case 2

For load case 2, the simulation for the MatLab model and AQWA are statistically analysed. By comparing the models results in table 5.2, it seems that for the motion of the tip of the TLB, the motions show similar behaviour for all three models. The maximum horizontal displacement is 0.35 m and vertical displacement is 0.65 m. This is small compared to the dimensions of the system.

X-direction [m]	μ	σ	$X_{1/3}$	X_{\max}
Single pendulum	-3.20E-05	0.094	0.189	0.35
Double Pendulum	-3.20E-05	0.094	0.189	0.35
AQWA	0	0.096	0.193	0.36

Z-direction [m]	μ	σ	$X_{1/3}$	X_{\max}
Single pendulum	-6.24E-05	0.172	0.34	0.64
Double Pendulum	-6.24E-05	0.172	0.34	0.64
AQWA	0	0.177	0.35	0.66

Table 5.2: Position of TLB tip

From the same simulation the horizontal and vertical motions of the COG of the jacket itself are given in table 5.3. The motions of the jacket are not very large, however there are quite some differences in the horizontal and vertical direction. From the vertical motion it is observed that the motions are that small, so that for future research this angle can be linearised. The standard deviation of the motion of the jacket in Z-direction is higher than for the pendulum models, while this is not the case for the X-direction. A possible explanation is the fact the the hoisting wires are elastic.

X-direction [m]	μ	σ	$X_{1/3}$	X_{\max}
Single pendulum	0.4410	0.1057	0.2114	0.3931
Double Pendulum	0.1925	0.0697	0.1394	0.2592
AQWA	1.0738	0.0852	0.1704	0.3408

Z-direction [m]	μ	σ	$X_{1/3}$	X_{\max}
Single pendulum	0.001	3.03E-04	6.06E-04	1.13E-03
Double Pendulum	2.54E-05	2.72E-05	5.45E-05	1.01E-04
AQWA	0.0059	3.50E-03	7.00E-03	1.30E-02

Table 5.3: Position of COG of jacket c.q. pendulum (lower) mass

In the pendulum models, the massless rods representing the hoisting wires are under a tension. By rearranging the equation of motions and filling in the simulation results, the tension at each time step for the MatLab model was found. From AQWA these tension can be extracted from the results file. The mean tension in all models are very close, namely $1.38 \cdot 10^8$ N . This value can be easily verified by calculating what the static tension is in the cable due the the weight of the jacket itself, as in equation 5.1.

$$T_{\text{static}} = M_{\text{jacket}}g = 14.000 \cdot 10^3 \cdot 9.81 = 1.373 \cdot 10^8 N \quad (5.1)$$

Equation 5.1 verifies that the tension is approximated well. However, significant differences in the oscillations are observed. The maximum value of the single and double pendulum is 13 and 5 times higher, respectively. One possible explanation is to do with the in-extensibility of the rod in de Matlab models. Due to the elasticity of the hoisting wires, the jacket in AQWA is allowed to extend the hoisting wires and move vertically. In the submerged part, this quadratic damping and buoyancy forces decrease the tensions amplitude in the hoisting wires.

Tension [N]	μ	σ	$X_{1/3}$	X_{\max}
Single pendulum	1.38E+08	1.29E+06	2.57E+06	4.78E+06
Double Pendulum	1.38E+08	5.44E+05	1.09E+06	2.02E+06
AQWA	1.35E+08	9.75E+04	1.92E+05	3.62E+05

Table 5.4: Tension in rod and hoisting wires

The interface between the jacket and the TLBs will be modelled as fenders, where kinetic energy must be absorbed in order to minimize impact (and damage) on the vessel. Therefore, the amount of amount of kinetic energy that needs to be absorbed is quadratically related to the in the relative velocity of the jacket and the TLBs. Since the motions of the vessel are independent of the motions of the jacket, the kinetic energy relative to the relative velocity has to fully dissipated by the interface between the jacket and the PS. The results from the analysis of the relative velocity is given in table 5.5.

X-direction [kg m/s]	μ	σ	$X_{1/3}$	X_{\max}
Single pendulum	3.4E+03	1.2E+06	2.5E+06	4.6E+06
Double Pendulum	3.4E+02	5.5E+05	1.1E+06	2.1E+06
AQWA	3.77E+03	9.51E+04	1.90E+05	3.54E+05

Z-direction [kg m/s]	μ	σ	$X_{1/3}$	X_{\max}
Single pendulum	3.30E+01	3.60E+03	7.20E+03	1.34E+04
Double Pendulum	9.29E+02	1.56E+05	3.11E+05	5.79E+05
AQWA	9.87E+03	6.86E+05	1.37E+06	2.55E+06

Table 5.5: Momentum of CoG

From tables 5.2 - 5.5, several observations are made:

- The tip of the TLBs has a maximum occurring deviation within a range of 1 meter. This is small relative to the dimensions of the system.
- Due to the small motions of the jacket, the impact between the jacket and the TLBs is will be induced by the tilting of the TLB. The tilting of the TLB will be achieved by pulling the derrick hoist wires with a velocity of 0.01 m/s. This would result in a horizontal velocity of the TLB tip of 0.0056 m/s. This velocity multiplied by the jacket mass would given an momentum of $p = 0.0056 \cdot 14.000.000 = 78400 \text{ kg m/s}$

If for each loadcase from table 2.5, the statistically maximum momentum of the jacket is calculated, the following results are obtained:

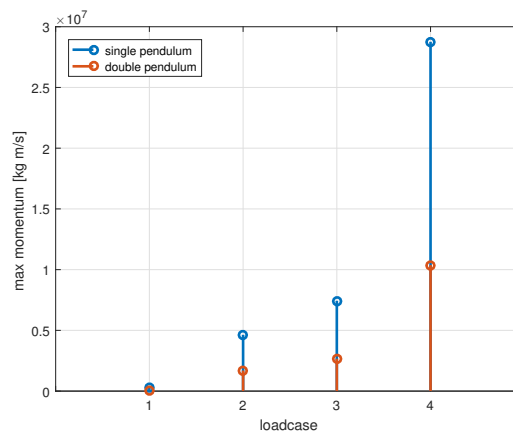


Figure 5.4: Maximum momentum per loadcase

Many simulations were conducted with the MatLab model of the submerged double and single pendulum. Though in general, the model showed the right behaviour within a certain range of the AQWA results, it was concluded that these models did not show consistent results enough in order to continue impact calculations. Therefore, for further calculations, the AQWA models are developed to model the actual impact and mating characteristics.

5.2. Impact

After simulation the motions of the free floating jacket, the tilting of the TLBs is applied, therefore causing impact at a certain point. To gain more insight in process impact, the velocity of the jacket is calculated. In impact mechanics, a measuring unit for impact is often the change in momentum [18], as explained in chapter 3. Therefore, in figure 5.5, the velocity of the jacket in the X, Z, θ direction can be seen for a still-water conditions.

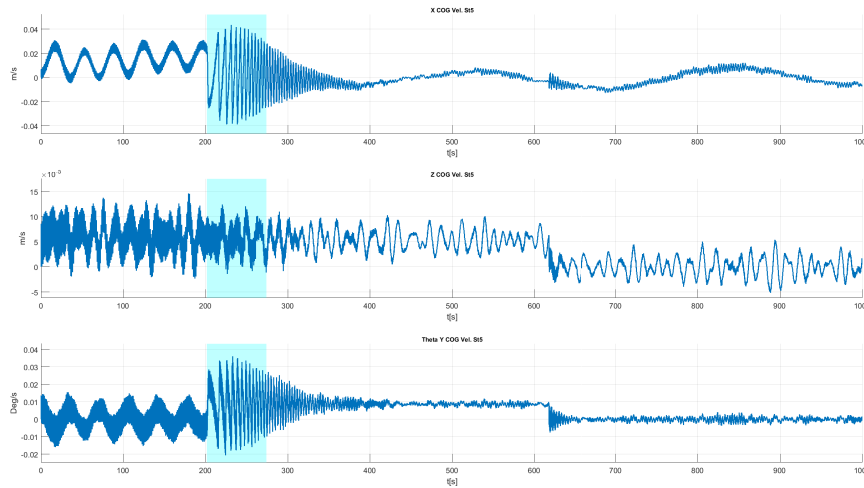


Figure 5.5: Structure motions without environment

In these figures, clearly the three phases can be observed; the suspended (free-hanging), transition and tilting phase. The transition phase is indicated by the cyan coloured part. The exact boundaries of these phases are determined with deflection of the fenders, because a clear distinction can be seen between contact and non-contact. This is more elaborately explained in section 5.2.2.

In all three different phases, a dominating frequency can be observed. Especially in the horizontal direction, these different frequencies can be distinguished. Therefore a spectral analysis is made from the horizontal motion in figure FFT, with the fast fourier transform. This can be seen in figure 5.6. The identified frequencies with a corresponding explanation is given in table 5.6.

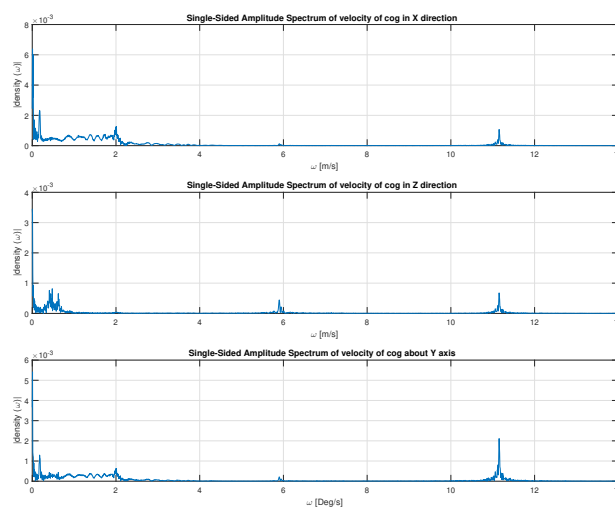


Figure 5.6: Spectral analysis of jacket velocity

Peak	Direction	Phase
0.006	x, θ	all
0.17	x, θ	free hanging
0.41-0.62	z	all
2.01	x, θ	tilt
5.9	z	free + transition
11.2	all	free + transition

Table 5.6: Spectral analysis results from figure 5.6

The following observations are made:

- Multiple peak can be seen in the range of the incoming wave spectrum.
- During free hanging phase: $\omega \approx 0.17$ rad/s.
- During the transition phase the frequency in still water conditions seems to increase from $\omega \approx 0.48$ rad/s to $\omega \approx 1.25$ rad/s
- During the tilting phase, slow varying harmonic motions are observed, with a frequency of $\omega \approx 0.02$ rad/s. This motions are not within the scope of this thesis, however, these motions are attributed to the low frequency mooring forces due to the slow varying drift.
- The higher peak are harder to explain. An initial presumption would be that it has something to do with the high stiffness of the cable configuration and the mass suspended from it. However, more extensive analysis is necessary to support this presumption.

In figure 5.7, the structure motions are given including environmental excitation of load case 2 (table 2.5)

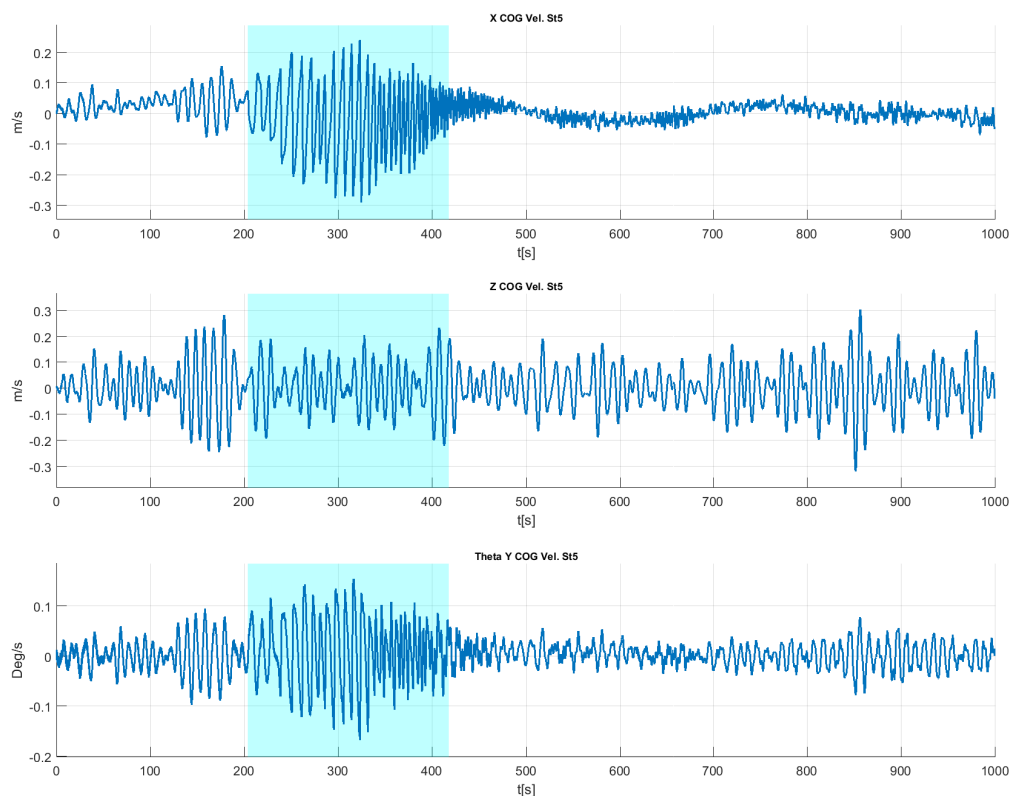


Figure 5.7: Structure motions with environment

A frequency analysis as in 5.6 shows that much more energy is present in the frequency part between 0 and 2 rad/s, due to the environmental actions.

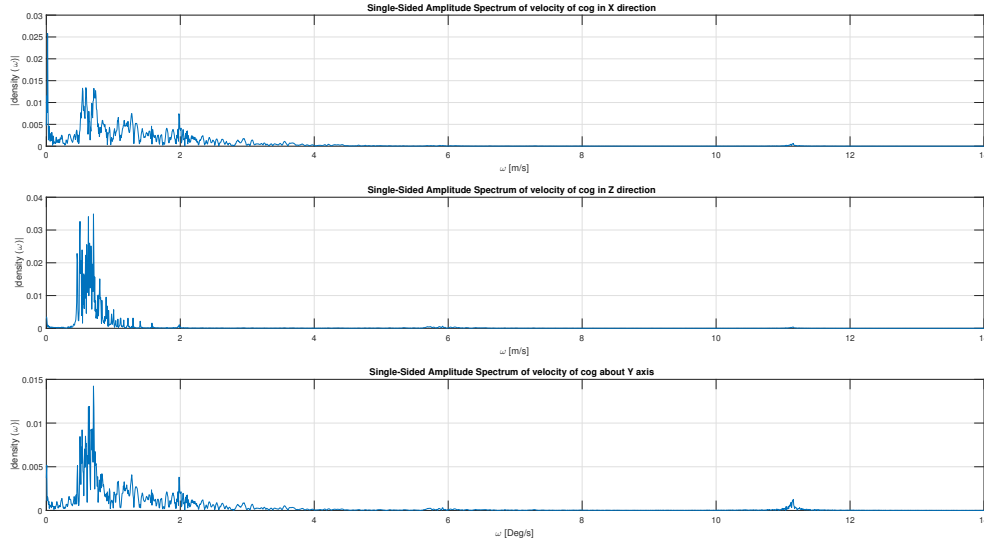


Figure 5.8: Spectral analysis of jacket velocity with environmental excitation

5.2.1. Static behaviour fender

Before looking at the dynamic analysis of the fenders, first the static forces of the fenders are considered. The jacket is in rest on the TLBs, and the full weight of the jacket is acts on the fenders. The total reaction force of these fenders are calculated as a function of tilting angle as in figure 5.9.

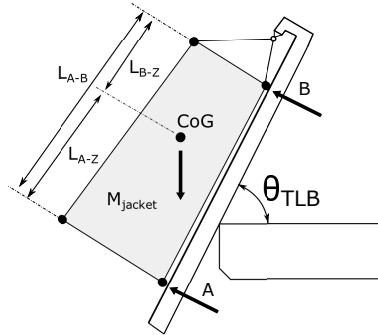


Figure 5.9: Static model for forces on fenders

The normal forces on the model are calculated with equations 5.2 - 5.4, in a rotated axis frame

$$\sum F = F_A + F_B - F_Z \cdot \cos\theta_{TLB} = 0 \quad (5.2)$$

$$\sum M_A = F_B \cdot L_{A-B} - F_Z \cos\theta_{TLB} \cdot L_{A-Z} = 0 \quad (5.3)$$

$$\sum M_B = -F_A \cdot L_{A-B} + F_Z \cos\theta_{TLB} \cdot L_{B-Z} = 0 \quad (5.4)$$

For the weight of the jacket, the dry weight is used. Equations 5.2 - 5.4 can be rewritten to:

$$F_A = \frac{L_{A-Z}}{L_{A-B}} M_{jacket} g \cdot \cos\theta_{TLB} \quad (5.5)$$

$$F_B = \frac{L_{B-Z}}{L_{A-B}} M_{jacket} g \cdot \cos\theta_{TLB} \quad (5.6)$$

Using the values from table 5.7, a graph is generated with reaction forces for both fenders in figure 5.10, for an angle range between $0 < \theta_{TLB} < 120$. However, it should be noted that now there are only 2 fenders taken per beam taking the impact. For negative forces, the fenders do not make contact, and is therefore 0.

	Value	Unit
M_{jacket}^a	7.000.000	kg
L_{A-B}	76.2	m
L_{A-Z}	26.5	m
L_{B-Z}	49.7	m

Table 5.7: Dimensions for static analysis

^aSince there are 2 beams, and it is assumed that the mass is evenly distributed over the two beams, the mass of the jacket is set at half of the total dry weight (14.000 tonnes)

As the weight distribution on both fenders changes as function of tilt, the fenders natural frequency change with it. It is calculated with:

$$\omega_n = \sqrt{\frac{k}{m}} = \sqrt{\frac{k}{F_{\text{fend}}/9.81}} \quad (5.7)$$

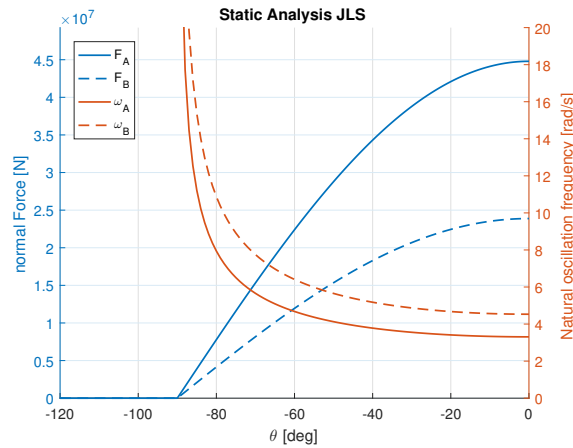


Figure 5.10: Normal forces fenders

5.2.2. No Environmental forces

First, a time domain simulation is run where the TLBs are hoisted in still water conditions, i.e. no environmental influences. The beams are hoisted with 0.01 m/s. The results can be seen in figure 5.11.

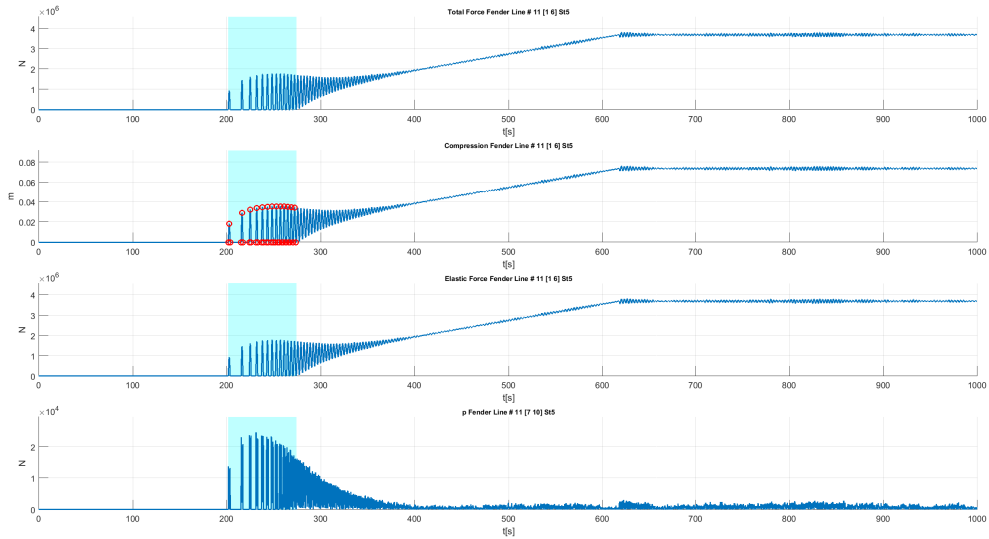


Figure 5.11: Fender forces without environmental influences

From this figure, several things can be observed.

- Three different phases can be observed; the suspended phase, the mating phase and the tilting phase. The transition from suspended phase tot mating phase is when the first compression occurs. In this case, this is at $t = 201$. The mating phase ends when there are no more occurrences of fender force reaching $F = 0$, indicating that there is no more contact. The exact point when these phases start and end are determined with these plots. The mating phase is highlighted in cyan in figure 5.11, and it's duration is $D_{\text{mating}} = 72s$.
- By analysing the data the amount of re-bounces can be calculated. In the compression graph, the start, maximum and end of impulse is marked with a red circles in 5.12. These values are corresponding with t_0 , t_c and t_f , respectively. The impulses, calculated with equation 3.77, can be seen in figure 5.13

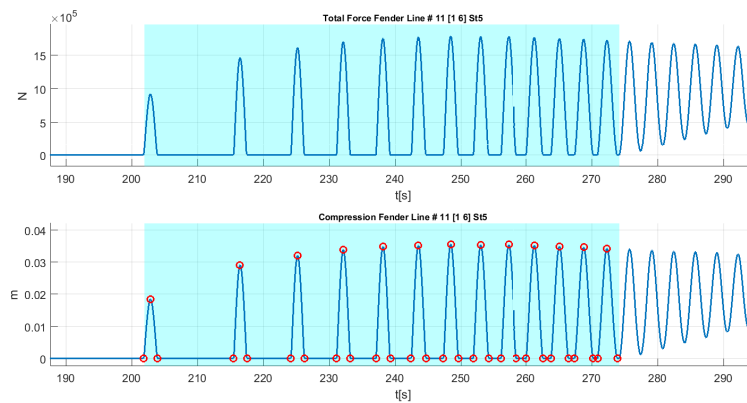


Figure 5.12: Detail of impact

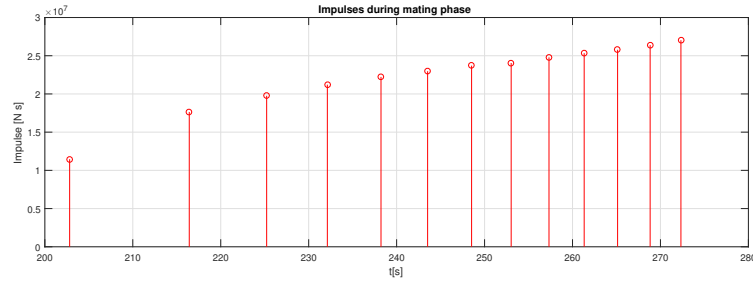


Figure 5.13: Impulses during mating phase

- The first impact is not the highest. The observation can be explained by the comparison of the system with a pendulum; the highest forces occurs when the jacket impact with the highest velocity. A pendulum has the highest velocity when it is a a zero angle position, and it has zero velocity in its outer position. The tilting of the TLBs causes the equilibrium point of the jacket closer to the fenders, therefore impact at higher velocity.
- After the mating phase, the tilting phase starts. During these phase, an increase can be observed in the compression as well in force. This is because the gravitational force on the fenders increases as the angle between the gravitational vector and normal vector of fender decreases.
- During the tilting phase, the fender seems the experience a harmonic motion, due to the springs. The frequency of this harmonic motion is identified as 1 rad/s.
- When zoomed in a single impact, for example the first at $t =$ in figure 5.14b, the damping coefficient shows the absolute damping force. However, during the decompression phase, the damping force is seems to make an inconsistent ‘jump’, whilst it should be negative. This is manually corrected, as in figure 5.14c.

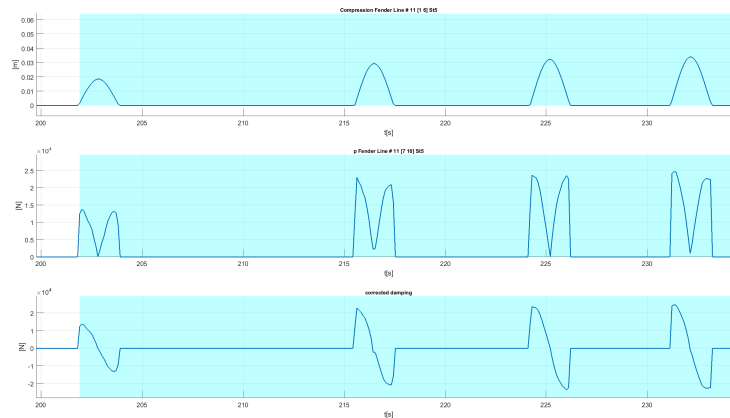


Figure 5.14: Detail of damping

- The derrick hoist is continually hoisting, until it reaches some arbitrarily chosen value, when it is certain in the tilting phase. When the hoisting stops, the jacket has a rotating inertia, that causes a short impulse on the fender system. This can be seen in figure 5.15. This effect is not within scope of this research and will be neglected.

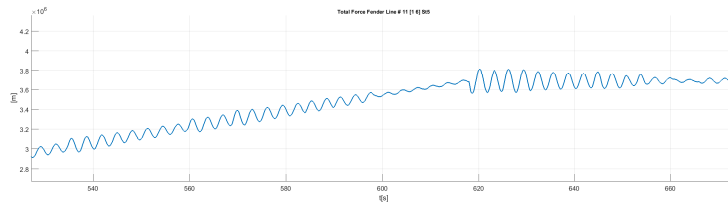


Figure 5.15: Detail of damping

- During this compressions phase, there should be not damping force at all, as the fender does not ‘stick’ to jacket. This is not implemented in the current model. Presumably, this damps the jacket motions even more in the model. However, this is recommended for future research.

5.2.3. With environmental forces

Now, the results of the simulation is given where the jacket and the vessel are excited by environmental forces. Load case 2 is applied (table 2.5). With a hoisting velocity of $\alpha_{TLB} = 0.01$ [m/s], this gives the results in figure 5.16

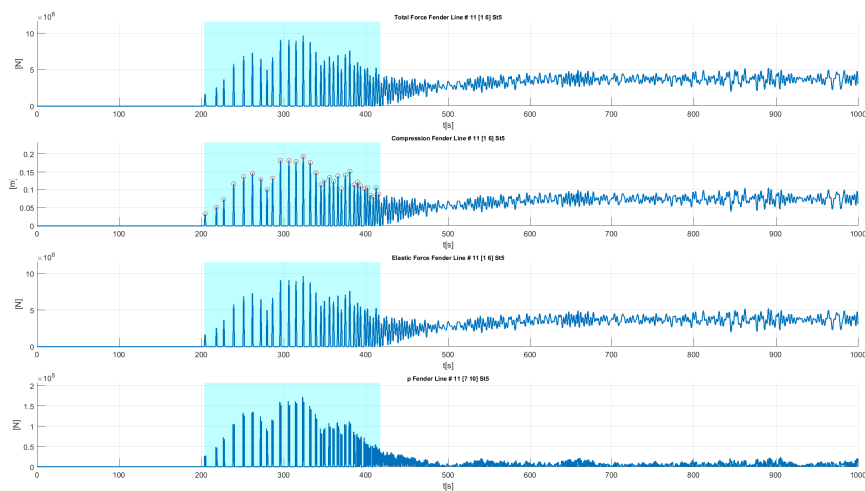


Figure 5.16: Fender forces with environmental influences

From these results, the following observations can be made:

- Environmental forces certain have an effect on the system. The duration of the mating phase increases, to $D_{\text{mating}} = 214$ s.
- Reboundes are much more frequent. In this load case, there are 31 re-bounces.

5.2.4. Maximum force vs H_s

In figure 5.19, the maximum force is plotted per significant wave height.

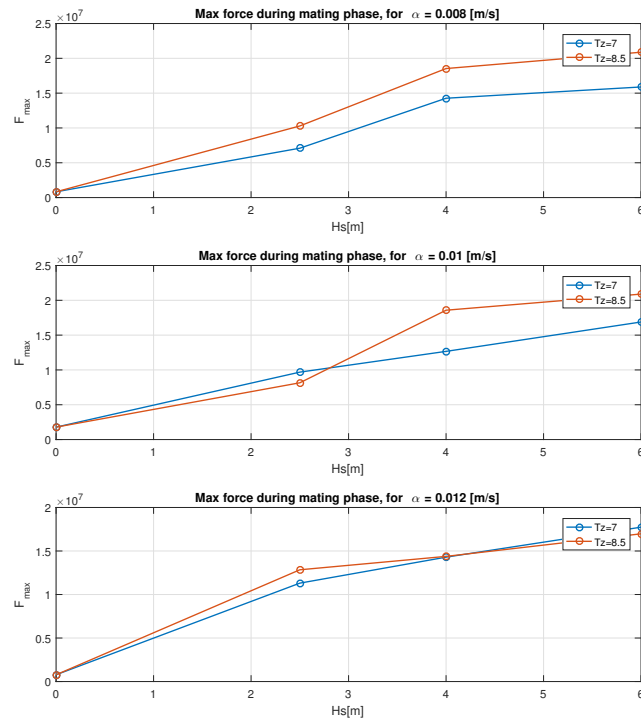


Figure 5.17: Maximum force vs H_s

The following observations can be made:

- At $H_s = 0$, the maximum force is obviously independent of T_z . However, with increasing tilting velocity, the maximum force is *higher* at $\alpha = 0.01$ m/s, but *lower* then *decreases* for $\alpha = 0.012$ m/s.
- For the design sea state, the maximum force is expected to be around 10 MN. To get a sense of magnitude, this force will be compared to the gravitational force the jacket exerts on the aft deck when the vessel is fully tilted and lying horizontally. In that case, the jacket is supported by all 8 support structures (only 4 experience impact during the transition phase). When the jacket is tilted until it is horizontal on the aft deck, each of the support structures will experience $\frac{1}{8}$ of the total gravitational force, i.e. 17 MN per support structure. Therefore, the designers of these jacket support structures should design for this maximum load and not for the impact during the transition phase.

5.2.5. Mating phase duration vs H_s

A batch simulation is done to check the sensitivity of the system to various environmental parameters. In tables 5.8 and 5.9 these results are given. The fender stiffness is $5 \cdot 10^7$ N/m and damping coefficient is 0.01. The tilting velocity is $\alpha_{TLB} = 0.01$ m/s. Per combination of H_s and T_p , 6 results are given: (in same order of appearance):

- Duration of mating phase [s]
- Maximum deflection of fender [m]
- Maximum force generated by fender [kN]
- Mean coefficient of restitution
- Mean impulse on jacket [kNs]
- Maximum impulse on jacket [kNs]
- Number of re-bounces.

H_s	0	2.5	4	6	
D_{mating}	72	214	232	708	[s]
$\delta_{\text{deflection}}$	0.036	0.193	0.253	0.336	[m]
F_{max}	1.78E+03	9.68E+03	1.27E+04	1.69E+04	[kN]
$e_{\text{✱}}$	0.811	1.150	1.285	2.080	[-]
\bar{p}	2.25E+04	2.25E+01	2.25E+01	2.25E+01	[kNs]
p_{max}	2.70E+04	1.51E+05	1.68E+05	4.17E+06	[kNs]
$N_{\text{rebounces}}$	13	31	30	67	[-]

Table 5.8: Results from simulation with $T_z = 6.8\text{s}$

H_s	0	2.5	4	6	
D_{mating}	72	232	265	656	[s]
$\delta_{\text{deflection}}$	0.036	0.163	0.370	0.337	[m]
F_{max}	1.78E+03	8.15E+03	1.86E+04	1.70E+04	[kN]
$e_{\text{✱}}$	0.811	1.656	1.174	1.627	[-]
\bar{p}	2.25E+04	7.04E+04	1.26E+05	4.46E+05	[kNs]
p_{max}	2.70E+04	3.35E+05	2.33E+05	1.27E+07	[kNs]
$N_{\text{rebounces}}$	13	35	26	40	[-]

Table 5.9: Results from simulation with $T_z = 8.5\text{s}$

The magnitude of all values increase with increasing environmental conditions. However, it appears that the duration of the mating phase increases exponentially between $H_s = 4$ and $H_s = 6$. This can be explained by examining the fender compression or force plot from that particular load case. Due to the more severe weather conditions, the fenders lose contact several more times after 200 seconds. When the mating phase duration is plotted against significant wave height and tilting velocity, the following graph (5.19). Especially for longer waves, the mating phase duration is less for higher tilting velocities. This can be explained by the fact that the jacket and beams' relative motion towards each other is faster, so that the steady state of continuous contact is made quicker.

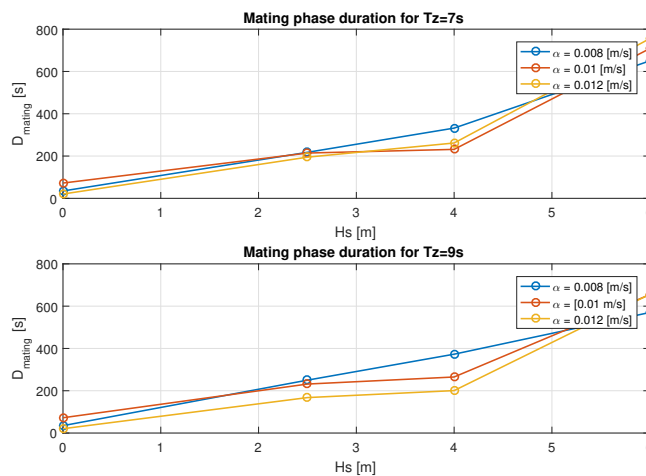


Figure 5.18: Maximum force vs H_s

5.3. Geometrical Loadcases

Besides the environmental parameters, also several geometrical parameters are varied, namely the tilting velocity α_{TLB} , fender stiffness and damping ratio

5.3.1. Number of re-bounces vs H_s

In figure 5.19 the number of re-bounces is shown for each of the different tilting velocities. One of the things that stands out is that at a tilting velocity of $\alpha_{TLB} = 0.01$ m/s, the amount of re bounces at still water conditions ($H_s = 0$) is higher than for $\alpha_{TLB} 0.008$ and 0.012 m/s. The main trend is that for an increasing severity of sea state, the amount of re-bounces increase. However, for $T_z = 8$.

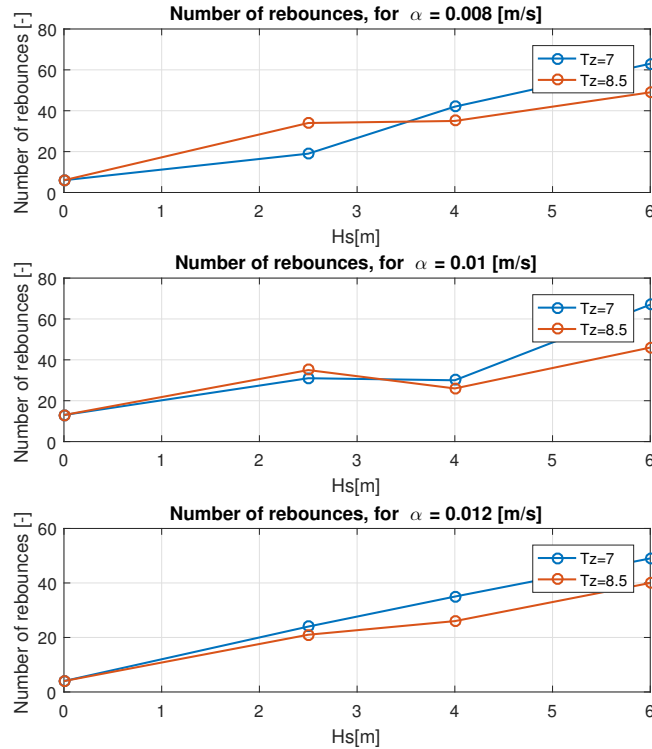


Figure 5.19: Maximum force vs H_s

5.3.2. Coefficient of Restitution

In figure 5.20, a graph of the compression in a fender is shown and the corresponding horizontal velocity of the jacket in X-direction. By determining the start (t_o) and end (t_f) and consequently dividing the corresponding velocities, the coefficient of restitution is obtained (equation 3.84). However, it should be noted that the jacket experiences a constant velocity due to the tilting of the jacket, which is independent of the collision. Conclusions drawn from change in this value should be done carefully.

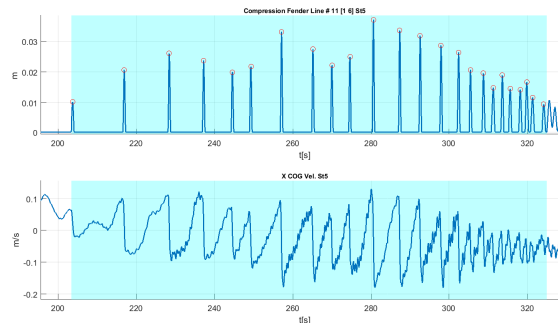


Figure 5.20: Jacket velocity vs at impact, for loadcase 2, with $k = 5E8$ N/m and $d = 0.01$

An overview of all responses calculated with the equations mentioned before can be found in tables 5.10 -

5.12, where fender parameters are varied, while environmental parameters are kept constant at the values of load case 2.

k	5.00E+03	5.00E+04	5.00E+05	[kN/m]
D_{mating}	200	258	186	[s]
$\delta_{\text{deflection}}$	0.618	0.168	0.034	[m]
F_{max}	3.09E+03	8.39E+03	1.72E+04	[kN]
e_{rebound}	1.413	1.297	2.319	[-]
\bar{p}	6.41E+03	6.39E+03	4.65E+03	[kNs]
p_{max}	9.26E+04	1.35E+05	1.39E+05	[kNs]
$N_{\text{rebounces}}$	19	50	55	[#]

Table 5.10: Result table for various geometrical parameters, for $d = 0.001$

k	5.00E+03	5.00E+04	5.00E+05	[kN/m]
D_{mating}	238	246	122	[s]
$\delta_{\text{deflection}}$	0.728	0.176	0.037	[m]
F_{max}	3.64E+03	8.79E+03	1.85E+04	[kN]
e_{rebound}	1.330	1.299	1.797	[-]
\bar{p}	7.12E+04	6.39E+04	4.55E+04	[kNs]
p_{max}	1.03E+05	9.92E+04	6.53E+04	[kNs]
$N_{\text{rebounces}}$	23	45	24	[#]

Table 5.11: Result table for various geometrical parameters, for $d = 0.01$

k	5.00E+03	5.00E+04	5.00E+05	[kN/m]
D_{mating}	161	120	73	[s]
$\delta_{\text{deflection}}$	0.431	0.084	0.018	[m]
F_{max}	2.16E+03	4.29E+03	1.04E+04	[kN]
e_{rebound}	2.488	1.146	1.166	[-]
\bar{p}	8.29E+03	5.80E+04	4.36E+04	[kNs]
p_{max}	2.66E+05	3.37E+05	1.65E+05	[kNs]
$N_{\text{rebounces}}$	11	14	11	[#]

Table 5.12: Result table for various geometrical parameters, for $d = 0.1$

From these tables, the following conclusions can be made:

- For increasing fender stiffness, the mating duration does only significantly decrease for $k = 5E8\text{N/m}$
- The mean coefficient of restitution increases for higher stiffness at $d = 0.001$, while for $d = 0.1$ this value decreases for higher stiffness. Due to the tilting of the beams, the jacket also obtains a velocity.

6

Conclusions

Numerical time-domain simulations of a jacket removal procedure have been conducted to research the behaviour of Allseas' Jacket Lift System. In this chapter, the conclusions and recommendations that follow from this thesis are presented.

6.1. Conclusions

3 models of the jacket lift system are developed. The first two are to predict the motions of a suspended jacket according to a single and double submerged pendulum model. In addition, a full 3D model of the jacket lift system was developed in ANSYS AQWA, to validate the pendulum. A direct-time domain simulation is used due to non-linear motions and forces, using a Runge-Kutta integration scheme. The hydrodynamic forces on the jacket are obtained by a instantaneous summation of Morison forces on all jacket members, where flow velocity and acceleration is calculated with potential flow. To accelerate simulations, the jacket is modelled as one cylinder with an equivalent diameter to account for drag and inertia.

In operational limit sea states, simulations showed that maximum occurring motions of the jacket are within a range of 1 meter in the horizontal direction, caused by predominantly drag forces, for all developed models. The actual mating of the jacket with the tilting lift beams is induced by the tilting of the beams. If there is no tilting, the beams will not make contact. In addition, the pendulum models do not take into account the disturbed fluid potential and dynamic positioning of the vessel. The pendulum models do not display the same behaviour as the 3D model and are therefore regarded to be insufficient to predict the mating of the jacket. Impact simulations were therefore conducted in the AQWA model.

The jacket mating loads are dependent on the kinetic energy that have to be absorbed by the jacket support structures. Fenders were modelled to absorb this energy, where values from typical fenders were used. The loads are dependent on the stiffness and size of the fender, i.e. possible deflection. From the motion analysis of the jacket, the most probable maximum momentum of the jacket is $3.5 \cdot 10^5$ kg m/s. This should be taken into account in the design of the jacket support structures.

A sensitivity analysis showed that the parameters that have most influence on the mating phase characteristics are the tilting velocity and the stiffness of the fender. The maximum occurring deflection will increase for increasing significant wave height, as that increases the momentum of the jacket. A higher wave period does not have an increasing influence on the maximum force.

When the jacket is tilted until it is horizontal on the aft deck, each of the support structure will experience a static force that is $\frac{1}{8}$ of the total gravitational force, i.e. 17 MN per structure. This load is critical and the designers of these jacket support structures should design for this maximum load and not for the impact during the transition phase.

With this information, the subquestions can now be answered:

- *How can both bodies, i.e. the jacket and the vessel, be described dynamically?*

3 models of the jacket lift system were developed. In 2 of these models the system was represented as

a single and double pendulum, with the jacket as a single cylinder with an equivalent drag and inertia diameter. In AQWA, the full 3D system is modelled. The pendulum models did not take into account all actions, of which most notably were wave drift forces on the vessel, wind and mooring (dynamic positioning). Therefore the absolute values are not usable for impact analyses, but it provides a good indication of the influences due to environmental actions.

- *How are these bodies coupled and how can this combined system be approximated by a model?*
In the pendulum representation, the motion of the jacket is assumed not to influence the motion of the vessel. In addition, the two structures are modelled connected with an inextensible rod. In the 3D model, the structures could influence each other, and the structures were connected with stiff cables. This adds an extra degree of freedom, resulting in different behaviour.
- *How can the jacket mating loads be approximated when the jacket makes contact with the vessel?*
The mating loads are dependent on the initial momentum of the jacket and the characteristics of the support structure. These structures have to absorb the total kinetic energy. By varying the stiffness and the deflection length, the maximum force could be approximated.
- *What are the most important external influences on the jacket lift system and how can these be integrated?*
Regarded as most important influences on the system are the environmental actions and the tilting of the beams, as they put energy in the system. The environmental load cases are based on the operating limits of the *Pioneering Spirit*, where the design load case is an Pierson-Moskowitz irregular sea with $H_s = 2.5$ m, $T_z = 5.7$ s and a current velocity of 0.5 m/s. In the AQWA model the tilting is integrated with a winch attached to the tilting lift beams, winching at 0.01 m/s. The influence of the environment proved to be of secondary importance.

With the answers presented above, the main research question is answered:

- ***What are the key influences on the dynamic behaviour of the jacket mating loads on the Pioneering Spirit during the transition phase.***
3 Models were developed, in order to predict the jacket motions and mating loads. From these models, it was derived that the most important parameters are fender stiffness and dimensions, and the tilting velocity. The fender characteristics determine the maximum energy absorption. The tilting velocity affects the time of contact during mating.
The sea state has a significant influence on the motion of the jacket. Increasing environmental conditions have an increasing effect on the most probable maximum momentum of the jacket, increasing the required energy absorption of the fenders.

6.2. Recommendations

- One aspect that has not been taken into account in calculating the response of the jacket is the presence and influence of the vessel on the linear fluid velocity potential. The fluid potential consists of the radiation potential, diffraction potentials and the incident undisturbed wave potential.

$$\Phi = \Phi_r + \Phi_d + \Phi_w \quad (6.1)$$

For the pendulum approach, the influence of vessel is only taken into account in the form of a prescribed imposed motion at the tip of the TLBs, and only the incoming undisturbed wave potential Φ_w is used. This assumption was necessary to build the pendulum model approach. The diffraction or radiation potentials might excite the system.

- The equivalent jacket model was used in order to accelerate the direct-time simulations. The approach is based on a method for bottom found offshore structures, by Dubbers et al [24]. However, this concerned a fixed structures on the sea bottom. A algorithm was written that automatically computes this equivalent jacket model, after which it remained in that form. However, in this case it concerned a jacket that is rotating and translating. If the rotation cannot be assumed as small, the equivalent model would have to be recalculated each time. In addition, the stick ranges would change and equivalent diameter for each specific range, adding up to the total computation time. Since the point was to decrease computational effort this is not done. Therefore, my recommendation would be to research whether this equivalent jacket model would still be valid for a moving truss structure.

List of Figures

1	Global vessel coordinate system	ix
2	Vessel motion coordinate system	ix
1.1	<i>Pioneering Spirit</i> with Johan Sverdrup topside (2018)	1
1.2	Layout of typical offshore structure	2
1.3	Schematic view of how the JLS works	2
1.4	Research methodology	4
2.1	<i>Pioneering Spirit</i> in JLS configuration	5
2.2	Schematic overview of Jacket Lift System	6
2.3	Location of jacket in North Sea	8
2.4	Jacket Properties	8
3.1	Pendulum model	11
3.2	Double Pendulum model	12
3.3	Wheeler stretching	17
3.4	Vector representation of single jacket member	18
3.5	Resulting moment around CoG	18
3.6	Pierson Moskowicz Spectrum	19
3.7	Phase lag difference	19
3.8	Time series wave height used for research	20
3.9	Impact mechanisms	21
3.10	Impact of a body and fender	22
3.11	Yokohoma pneumatic fender	23
4.1	Simplified sketch of model	25
4.2	Response Amplitude Operator of the PS	27
4.3	Heave motion of different positions	27
4.4	Heave acceleration of different positions	27
4.5	Point mass locations on PS	28
4.6	Difference RAOs of the PS	28
4.7	Mass Spring system	29
4.8	Drag coefficient [12]	30
4.9	Force profile on jacket	31
4.10	Graphical representation of equivalent stick-model method [24]	32
4.11	Force profile on equivalent jacket	32
4.12	Force profile on single cylinder representation of jacket	33
4.13	AQWA Model of jacket	33
4.14	AQWA Model of <i>PS</i>	33
4.15	AQWA model PS with Forties C Jacket	34
4.16	AQWA model PS with rotated jacket from side	35
5.1	Surge motion load case 2, single pendulum	38
5.2	Surge motion load case 2, double pendulum	38
5.3	AQWA Simulation Surge motion load case 2	38
5.4	Maximum momentum per loadcase	40
5.5	Structure motions without environment	41
5.6	Spectral analysis of jacket velocity	41
5.7	Structure motions with environment	42

5.8 Spectral analysis of jacket velocity with environmental excitation	43
5.9 Static model for forces on fenders	43
5.10 Normal forces fenders	44
5.11 Fender forces without environmental influences	45
5.12 Detail of impact	45
5.13 Impulses during mating phase	46
5.14 Detail of damping	46
5.15 Detail of damping	47
5.16 Fender forces with environmental influences	47
5.17 Maximum force vs H_s	48
5.18 Maximum force vs H_s	49
5.19 Maximum force vs H_s	50
5.20 Jacket velocity vs at impact, for loadcase 2, with $k = 5E8$ N/m and $d = 0.01$	50
6.1 Surge motion load case 1, single pendulum	61
6.2 Surge motion load case 1, double pendulum	61
6.3 Surge motion load case 2, single pendulum	62
6.4 Surge motion load case 2, double pendulum	62
6.5 Surge motion load case 3, single pendulum	62
6.6 Surge motion load case 3, double pendulum	63
6.7 Surge motion load case 4, single pendulum	63
6.8 Surge motion load case 4, double pendulum	63
6.9 Performance curve of Yokohama pneumatic fender [$p_0 = 50$ kPa]	65
6.10 Performance curve of Yokohama pneumatic fender [$p_0 = 80$ kPa]	66
6.11 Single Cylinder Morison forces	70
6.12 Single Cylinder Morison forces	70
6.13 Single Cylinder Morison forces - AQWA Model	71
6.14 MatLab - AQWA Verification	72

List of Tables

2.1	General dimension <i>Pioneering Spirit</i>	5
2.2	TLB Centre of Gravity	7
2.3	Lift operations conditions	7
2.4	Operational limit JLS	9
2.5	Environmental load cases	9
4.1	Pendulum dimensions	26
4.2	Point mass locations	28
4.3	Measuring locations	35
5.1	Environmental load cases	37
5.2	Position of TLB tip	39
5.3	Position of COG of jacket c.q. pendulum (lower) mass	39
5.4	Tension in rod and hoisting wires	39
5.5	Momentum of CoG	40
5.6	Spectral analysis results from figure 5.6	42
5.7	Dimensions for static analysis	44
5.8	Results from simulation with $T_z = 6.8s$	49
5.9	Results from simulation with $T_z = 8.5s$	49
5.10	Result table for various geometrical parameters, for $d = 0.001$	51
5.11	Result table for various geometrical parameters, for $d = 0.01$	51
5.12	Result table for various geometrical parameters, for $d = 0.1$	51
6.1	Typical values for Yokohama type pneumatic fenders with $p_0 = 50$ kpa [26]	65
6.2	Typical values for Yokohama type pneumatic fenders with $p_0 = 80$ kpa [26]	65
6.3	Simulation settings for single fixed cylinder	69

Appendix A: Personal information

Institution

Delft University of Technology
Faculty of 3mE
Offshore & Dredging Engineering Department
Mekelweg 2
2628 CD Delft, the Netherlands

Company

Allseas Engineering B.V.
Innovations Department
Poortweg 12
2612 PA Delft, The Netherlands
<http://www.allseas.com>

Author

Edward (Ward) R. Kuiters
Prins Hendrikstraat 125
2518 HN The Hague, the Netherlands
e.r.kuiters@gmail.com

Graduation committee members

Prof.dr.ir. A.P. van 't Veer
Maritime and Transport Technology Department, Delft University of Technology
Riaan.vantVeer@tudelft.nl

Dr.ir. P.R. Wellens
Maritime and Transport Technology Department, Delft University of Technology
P.R.Wellens@tudelft.nl

Ir. H. Bailly Guimaraes
Naval Architect, Innovations department, Allseas Engineering
HBG@Allseas.com

Dr.ir. A. Vrijdag
Maritime and Transport Technology Department, Delft University of Technology
A.Vrijdag@tudelft.nl

Appendix B: Simulation results

6.3. Load case 1

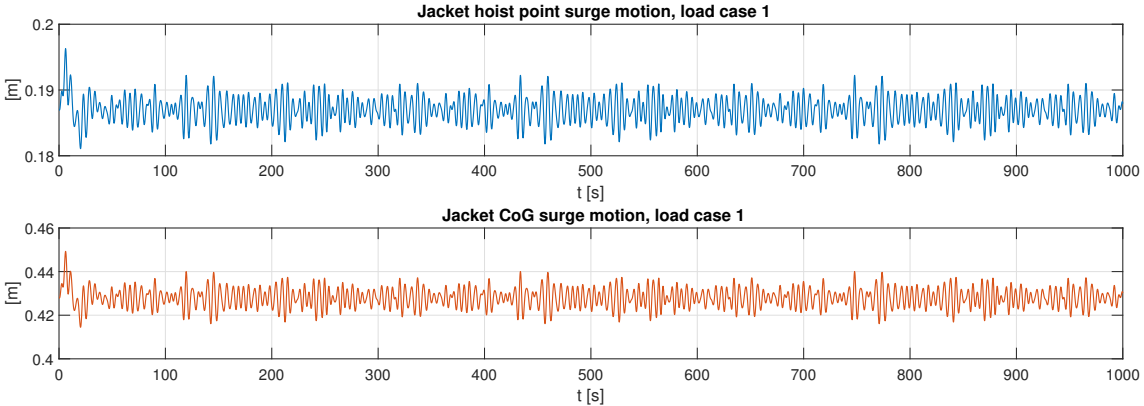


Figure 6.1: Surge motion load case 1, single pendulum

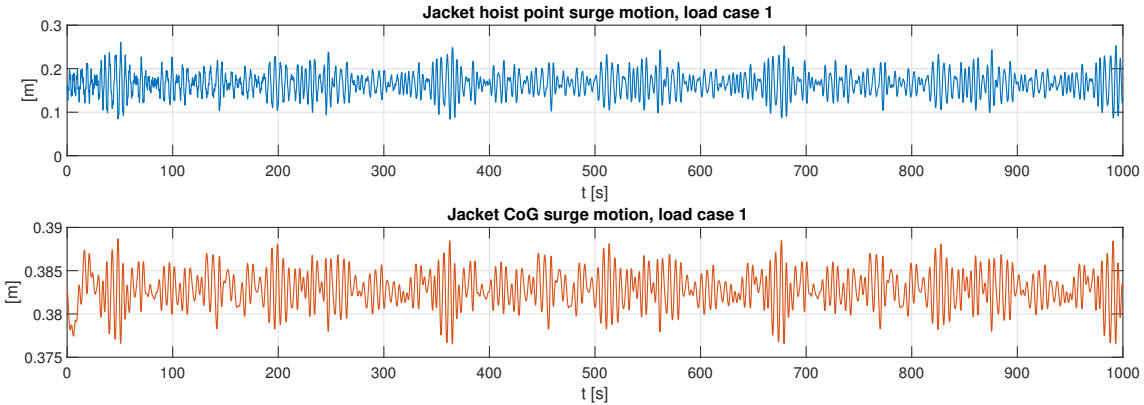


Figure 6.2: Surge motion load case 1, double pendulum

6.4. Load case 2

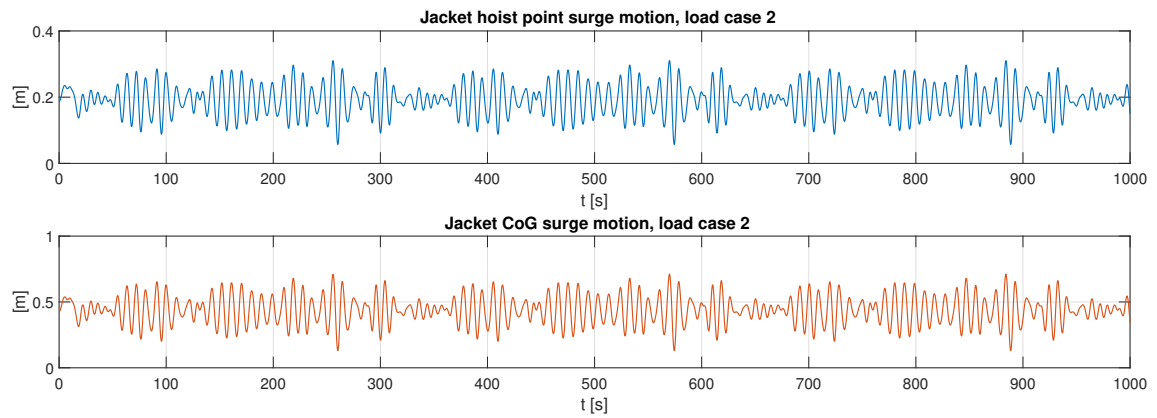


Figure 6.3: Surge motion load case 2, single pendulum

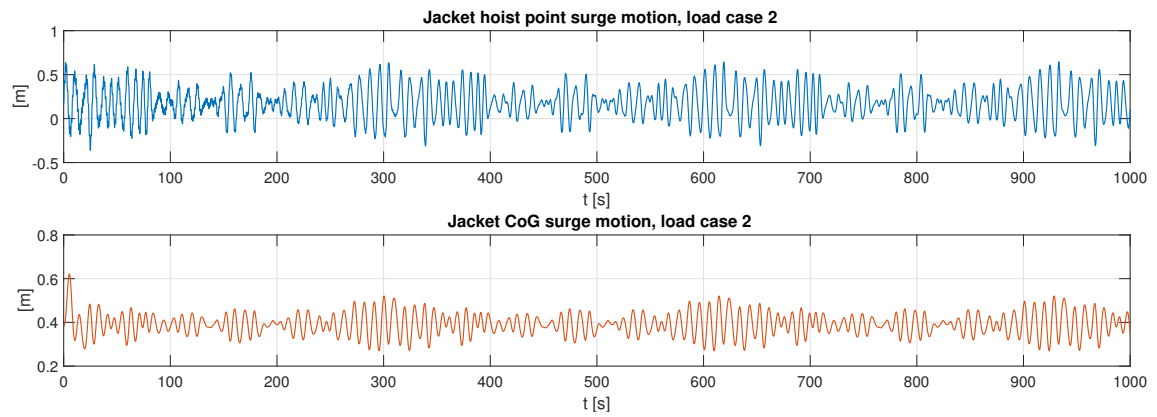


Figure 6.4: Surge motion load case 2, double pendulum

6.5. Load case 3

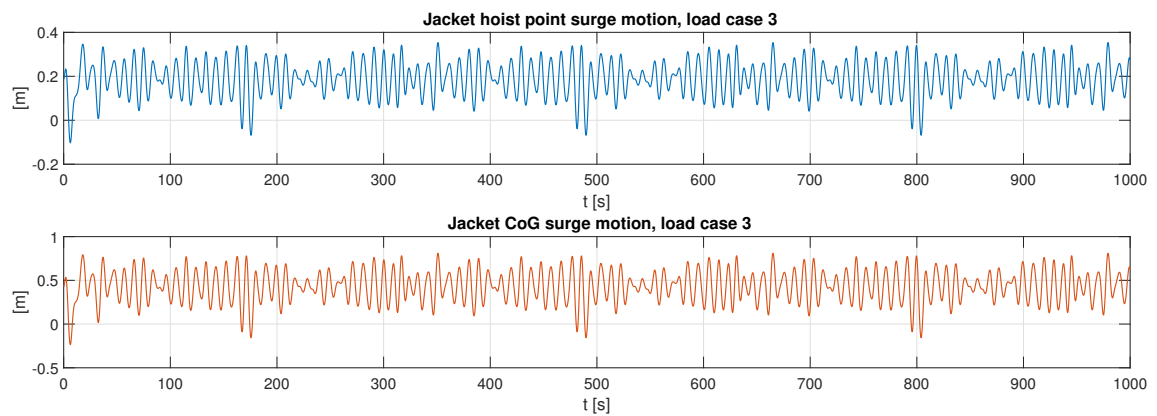


Figure 6.5: Surge motion load case 3, single pendulum

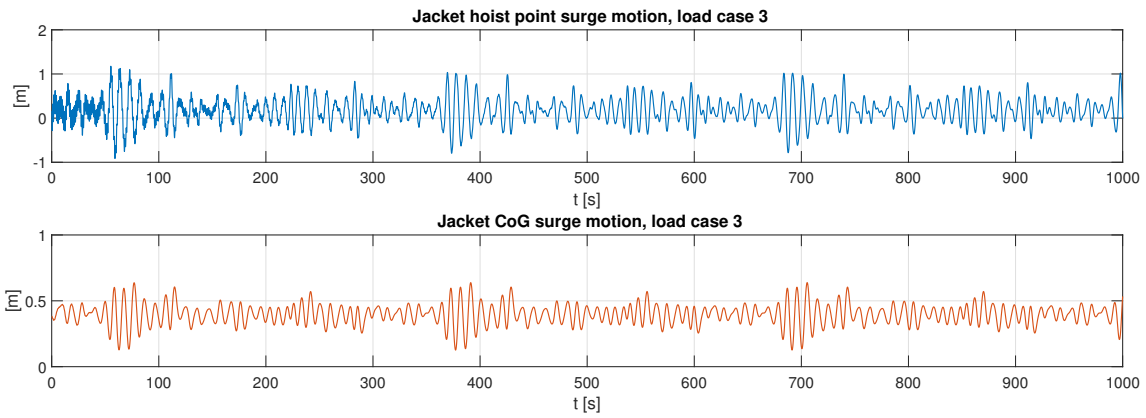


Figure 6.6: Surge motion load case 3, double pendulum

6.6. Load case 4

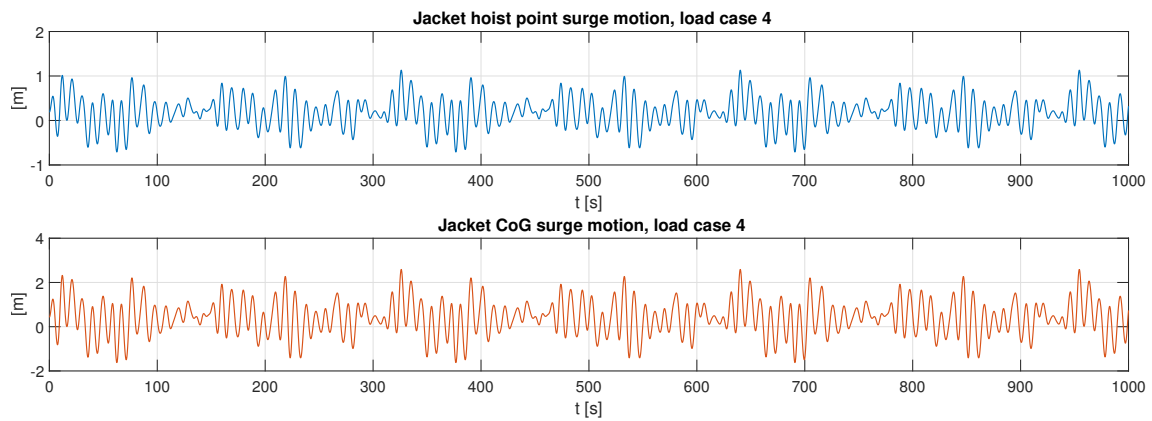


Figure 6.7: Surge motion load case 4, single pendulum

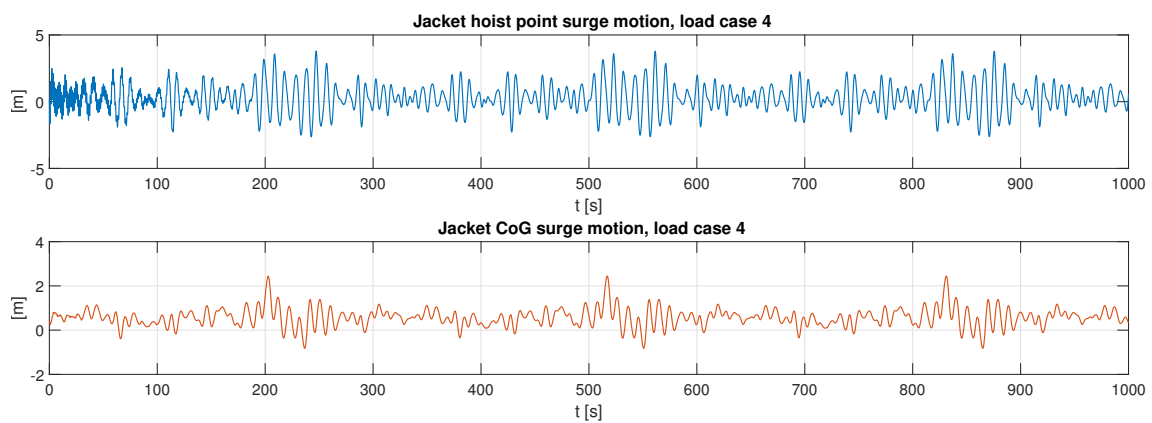


Figure 6.8: Surge motion load case 4, double pendulum

Appendix C: Fender characteristics

Nominal size (Diameter x Length) [mm]	Initial pressure [kPa]	Internal pressure [kPa]	Guaranteed Absorption (GEA) [kJNm]	Energy [kJNm]	Reaction force at GEA [kN]
1500x3000		50		153	579
2500x5500		50		943	2019
4500x12000		50		6473	7984

Table 6.1: Typical values for Yokohama type pneumatic fenders with $p_0 = 50$ kpa [26]

Nominal size (Diameter x Length) [mm]	Initial pressure [kPa]	Internal pressure [kPa]	Guaranteed Absorption (GEA) [kJNm]	Energy [kJNm]	Reaction force at GEA [kN]
1500x3000		80		214	761
2500x5500		80		1317	2653
4500x12000		80		9037	10490

Table 6.2: Typical values for Yokohama type pneumatic fenders with $p_0 = 80$ kpa [26]

In graph 6.9 and 6.10, the performance curve of the largest types of Yokohama fenders are given. A performance curve, or load-deflection curve gives a rough indication of the fender behaviour under loading. The initial pressure p_0 affect the behaviour, therefore two similar types are given with different initial pressure.

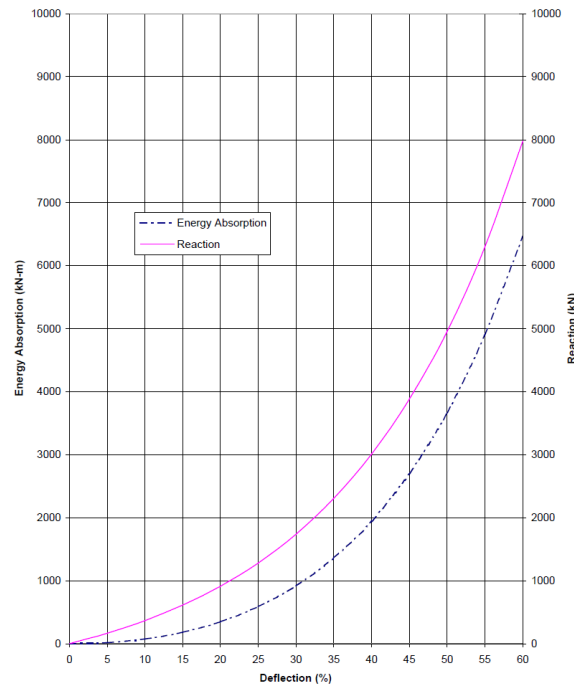


Figure 6.9: Performance curve of Yokohama pneumatic fender [$p_0 = 50$ kPa]

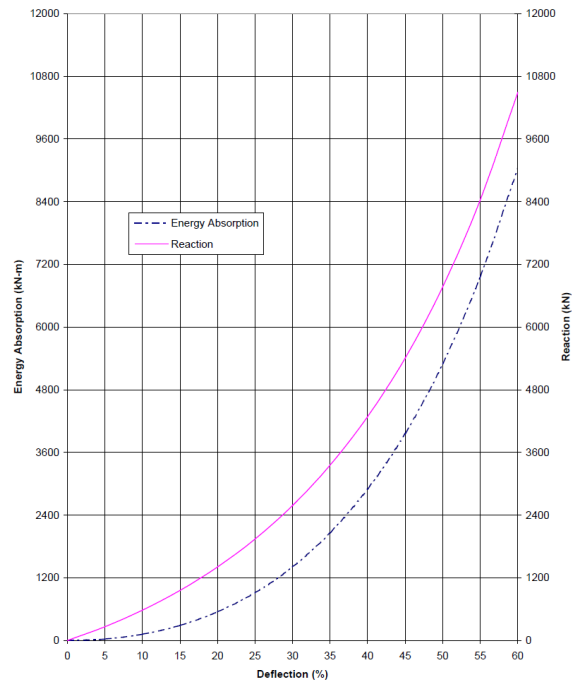


Figure 6.10: Performance curve of Yokohama pneumatic fender [$p_0 = 80$ kPa]

Appendix E: MatLab model verification

In order to verify calculation of the Morison function of equation 3.38 work, several comparisons are made. The AQWA model is compared with the MatLab model, as well as that the MatLab model is run with varying settings.

The design jacket is a large and complex structure, where for each time step, many vector calculations and integrations take place to calculate the Morison forces. To verify the Morison calculation, the jacket is replaced by a **single fixed** submerged tube in infinite depth. The settings from table 6.3 apply:

Item	Value	Unit	Description
Length	5	m	Length of cylinder
Diameter	0.2	m	Diameter of cylinder
Water depth	1000	m	Waterdept at location of cylinder
Distance top to MSWL	5	m	For fully submersion
H_s	2.5	m	Waveheight
ω	1	rad/s	Frequency (Period $T = 6.28$ s)
u_{curr}	0.5	m/s	Current velocity
C_d	1.08	-	Drag Coefficient
C_m	1.2	-	Inertia coefficient
Max element size	0.05	m	Element size for discrete time integration
Time step	0.001	s	Time step
Simulation time	30	s	Total simulation time

Table 6.3: Simulation settings for single fixed cylinder

First, only the effect of current is researched. Therefore, there are only drag forces and no inertia forces on the cylinder. The current is not dependent on the vertical coordinate, therefore it can be left out the integral in equation 6.2. With equation 6.3 the total force is calculated to be 138.4 N . In figure 6.11 the output of the model is found; it can be seen that this indeed the calculated with the model.

$$F_{\text{drag, current}} = 0.5\rho C_d D \cdot \int_{L_{\min}}^{L_{\max}} u_{\text{curr}}^2 dz \quad (6.2)$$

$$= 0.5 \cdot 1025 \cdot 1.08 \cdot 0.5^2 \cdot 5 = 138.4 N \quad (6.3)$$

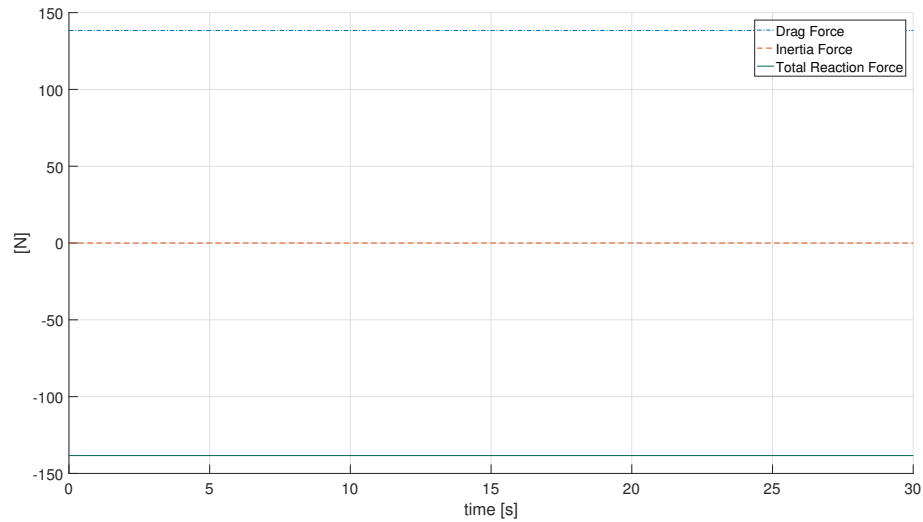


Figure 6.11: Single Cylinder Morison forces

The Morison forces force on the cylinder due to a regular wave is calculated.. A regular wave with $H = 2.5$, $T = ..$ is acting on the jacket. The environmental part is plotted in figure 6.12.

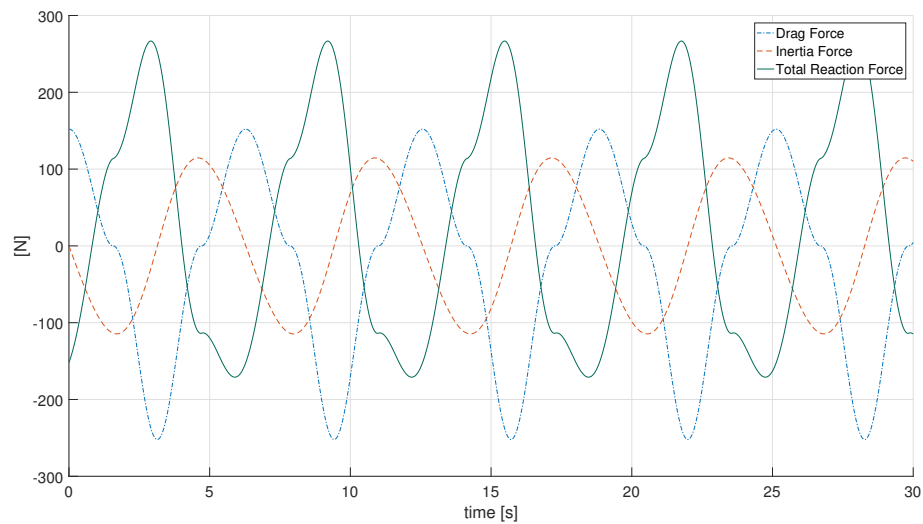


Figure 6.12: Single Cylinder Morison forces

To check whether this is true, the peak of the drag and inertia is calculated. This is done in equations 6.6-6.9

$$F_{I,\max} = \int_{L_{\min}}^{L_{\max}} \frac{\pi}{4} \rho C_M D^2 \cdot \dot{u}_{\max} dz \quad (6.4)$$

$$= \frac{\pi}{4} \rho C_M D^2 \cdot \zeta_a k g \cdot \int_{L_{\min}}^{L_{\max}} e^{kz} dz \quad (6.5)$$

$$= \frac{\pi}{4} \rho C_M D^2 \cdot \zeta_a g \cdot e^{kz} \Big|_{L_{\min}}^{L_{\max}} = 113N \quad (6.6)$$

$$F_{d,max} = \int_{L_{min}}^{L_{max}} \frac{1}{2} \rho C_d D \cdot u_{max} |u_{max}| dz \quad (6.7)$$

$$= \frac{1}{2} \rho C_d D \cdot \left(\zeta_a \frac{kg}{\omega} \right)^2 \cdot \int_{L_{min}}^{L_{max}} e^{2kz} dz \quad (6.8)$$

$$= \frac{1}{2} \rho C_d D \cdot \left(\frac{kg}{\omega} \right)^2 \frac{1}{2k} \cdot e^{2kz} \Big|_{L_{min}}^{L_{max}} = 195N \quad (6.9)$$

These forces correspond to the output of the model in figure 6.12. The chosen wave period, 6.28 s, corresponds with the harmonic motions in the graph. Also, the inertia force lags a half phase behind the drag force, which is logical due to the fact that acceleration lags a quarter period behind velocity for sinusoidal motions.

AQWA Model verification

The same model verification as for the MatLab model was done for AQWA. In figure 6.13, a very similar results graph can be seen as with figure 6.12. The drag and inertia forces are in the same order magnitude as for the MatLab model. In this case, Aqwa-Naut was applied since it concerned a regular wave.

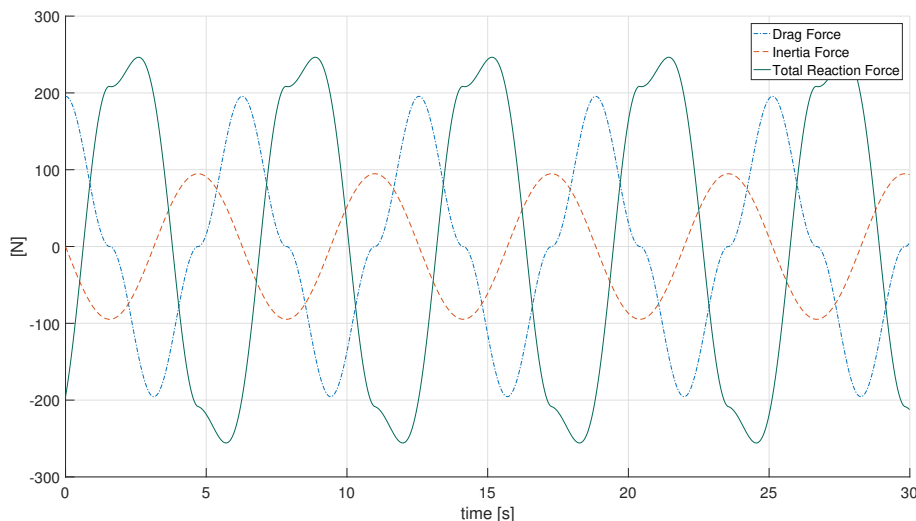
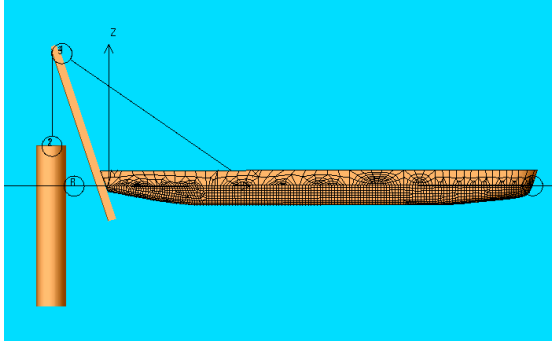


Figure 6.13: Single Cylinder Morison forces - AQWA Model

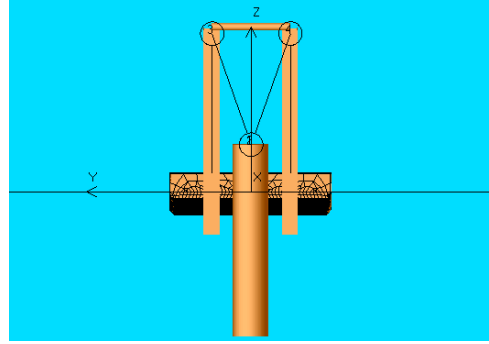
In addition, a model in AQWA was made the 3D AQWA model and 2D pendulum Matlab comparable. In AQWA, instead of a fully defined jacket, a single cylinder was made. The height of the cylinder is twice the length between the top of the jacket and the CoG. This is a discrepancy with real jacket, but a cylinder in AQWA has its CoG per definition in the middle, whilst the jacket CoG is lower than the geometrical middle. The material density of the jacket is scaled¹ in order to match the weight of the jacket. The cylinder has an arbitrarily chosen thickness of 20cm.

The Matlab model is in the X-Z plane. Therefore, in the AQWA model, translation in the Y-direction and rotation around the X and Z axis are locked for all structures. Two jacket hoisting wires, attached to the top centre of the cylinder, are set as very stiff ($k = 6 \cdot 10^8$) in order to approximate the inextensible rod from the Matlab model. The model can be seen in figure 6.14a and 6.14b from aft view.

¹An initial AQWA-Line simulation was conducted. Consequently, the weight extracted from the result file was divided with the actual jacket weight of 14.000 tonnes. This factor was multiplied with the material density of cylinder material



(a) PS with equivalent cylinder



(b) PS with equivalent cylinder, aft view

Figure 6.14: MatLab - AQWA Verification

Bibliography

- [1] OSPAR Convention for the Protection of the Marine Environment of the North-East Atlantic, September 1992.
- [2] F. Wasser, "Pieter Schelte jacket lift system, a dynamic analysis of the initial lifting phase," Master's thesis, Delft University of Technology, March 2010.
- [3] M. L. G.S. Grewal, "Ship impact on offshore minimum structure platforms," pp. 3–13, 2009.
- [4] Allseas, "Operational procedure jacket removal." Internal document, 2013.
- [5] Allseas, "Jls design jackets weight and CoG." Internal document, August 2017.
- [6] R. Kwiatkowski, "Dynamic analysis of double pendulum with variable mass and initial velocities," *Procedia Engineering*, vol. 136, pp. 175–180, 2016.
- [7] J. Awrejcewicz, *Classical Mechanics*. Springer, 2012.
- [8] E. Moore, "Runge-Kutta Formulae," 1974.
- [9] L. H. Holthuijsen, *Waves in Oceanic and Coastal Waters*. Cambridge, 2007.
- [10] T. F. Ogilvie, "First- and second-order forces on a cylinder submerged under a free surface," *Journal of fluid mechanics*, vol. 16 (3), pp. 451–472, 1963.
- [11] S. S. J. Morison, J. Johnson, "The force exerted by surface waves on piles," *Journal of Petroleum Engineering*, vol. 2 (5), pp. 149–154, 1950.
- [12] DNV, "Environmental conditions and environmental loads, dnv-rp-c205," tech. rep., Det Norske Veritas, April 2007.
- [13] W. M. J.M.J. Journée and R. Huijsmans, *Offshore Hydromechanics; third edition (2015)*. Delft University of Technology, 2000.
- [14] D. C. Lay, *Linear Algebra and Its Applications*. Pearson - Addison Wesley, 2006.
- [15] L. Blok, J.J.; Brozius and J. Dekker, "The impact loads of ships colliding with fixed structures," 1983.
- [16] Y. Khulief, "Modeling of impact in multibody systems: An overview," *Journal of Computational and Nonlinear Dynamics*, vol. 8, April 2013.
- [17] S. H. M. Nagurka, "A mass-spring-damper model of a bouncing ball," 2004.
- [18] W. Stronge, *Impact Mechanics*. Cambridge University Press, 2000.
- [19] G. B. A. Jönsson, J. Bathelt, "Implications of modelling one-dimensional impact by using a spring and damper element," *Proceedings of the Institution of Mechanical Engineers*, October 2004.
- [20] J. W. Gaythwaite, *Design of Marine Facilities for the Berthing, Mooring and Repair of Vessels, second edition*. American Society of Civil Engineers, 2004.
- [21] *Study on the vibratory roller-ground interaction and its application to the control of a roller*, Proceedings of 5th Asian Pacific Regional Conference International Society for Terrain-Vehicle Systems, October 1998.
- [22] D. n. G. Nesar, "Dynamics of ships and fenders during berthing in a time domain," *Ocean Engineering*, 2006.

-
- [23] L. H. C. G H Keulegan, "Forces on cylinders and plates in an oscillating fluid," *Journal of Research of the National Bureau of Standards*, vol. Vol 60, no. No 5, May 1958.
- [24] R. Dubbers and J. Hoving, "OE44095 hand-out: The equivalent stick-model reviewed." Original by Dubbers (2004), revisions by JS Hoving with help of S.W.G. Huiskes, 2014-2016.
- [25] L. E. Borgman, "Random hydrodynamic forces on objects," *The Annals of Mathematical Statistics*, vol. Vol. 38, no. No.1, pp. 37-51, February 1967.
- [26] "Yokohama pneumatic fender leaflet." <https://www.fendercare.com/marine-products/floating-fenders/yokohama-pneumatic-floating-fenders/>. Accessed: 2018-05-30.

